ELSEVIER

Nuclear Physics A 640 (1998) 163–195

NUCLEAR PHYSICS A

Structure of excited bands in ^{162}Tm and residual interactions

J.M. Espino [a], G.B. Hagemann [b], I.G. Bearden [b], R.A. Bark [b,1], M. Bergström [b], A. Bracco [c], B. Herskind [b], H.J. Jensen [b], S. Leoni [c], C. Martínez-Torre [a], B. Million [c], P.O. Tjøm [d]

[a] *Facultad de Física, Universidad de Sevilla, Apdo. 1065, E-41080 Sevilla, Spain*

[b] *Niels Bohr Institute, University of Copenhagen, Tandem Accelerator Laboratory, DK-4000 Roskilde, Denmark*

[c] *Instituto Nazionale di Fisica Nucleare, Milan, Italy*

[d] *Department of Physics, University of Oslo, Oslo, Norway*

Received 29 April 1998; revised 15 June 1998; accepted 1 July 1998

Abstract

The nucleus ^{162}Tm has been populated by the ^{130}Te(^{37}Cl,5n) reaction, and the γ-cascades detected with the NORDBALL array. Eight coupled rotational bands involving the proton orbitals, $g_{7/2}[404]7/2^+$, $d_{3/2}[411]1/2^+$, $d_{5/2}[402]5/2^+$, $h_{11/2}[523]7/2^-$ and $h_{9/2}[541]1/2^-$ and neutron orbitals $i_{13/2}[642]5/2^+$, $h_{9/2}[523]5/2^-$ and $f_{7/2}[521]3/2^-$ have been established in ^{162}Tm, to spins varying from 18 to 47$\hbar$. Various phenomena which can be related to residual neutron–proton interactions are discussed. In particular, signature inversion in the $\pi[541]1/2^- \otimes \nu[642]5/2^+$ bands based on the $h_{9/2}$ quasiproton and $i_{13/2}$ quasineutron, respectively, may be explained by a fairly large p–n interaction. In addition, interactions at the crossings of bands with constituent quasiparticles differing both in parity and signature have been extracted with strength of the order of a few (4–12) keV. Such interactions also require terms beyond the standard mean field description. © 1998 Elsevier Science B.V.

PACS: 21.10.-k; 23.20.Lv; 25.70.-z; 27.70.+q

Keywords: NUCLEAR REACTIONS ^{130}Te(^{37}Cl,5n)^{162}Tm, E = 166 MeV; measured E_γ, I_γ, $\gamma\gamma$ coin., deduced levels. J, π rotational band structure, configurations, alignments, $B(M1)/B(E2)$ ratios, $B(E1)$ values, crossing frequencies. Signature inversion, interaction strengths, proton–neutron interactions.

[1] Present address: Department of Nuclear Physics, Research School of Physical Sciences and Engineering, The Australian National University, Canberra ACT 0200, Australia.

PII S0375-9474(98)00433-3

1. Introduction

In odd–odd nuclei there is a multitude of possible combinations of quasineutrons and quasiprotons forming the band structures, at low excitation energy. If all these bands can be assigned spin and parity and interpreted in terms of relevant configurations there are rich possibilities of studying nuclear structure phenomena particular to odd–odd nuclei. By drawing on spectroscopic information in neighbouring even–even and odd nuclei information on residual proton–neutron interactions may also be addressed.

In the present experiment we have extended the level scheme of ^{162}Tm to 16 bands characterized by a given signature. It has been possible to firmly determine spins, parities and excitation energies associated with these bands, relative to a known 5^+ isomeric state, except for one pair for which an unobserved low-energy transition introduces an uncertainty. These data form an excellent basis for a comparison to Cranked Shell Model predictions. Extraction of residual interactions of various forms are also attempted.

2. Experimental methods and data analysis

The data analysed in the present work were taken in two separate experiments, using the accelerator facility of the Niels Bohr Institute and the Nordball spectrometer [1]. In both cases, the nucleus ^{162}Tm was populated up to high spins with the reaction ^{130}Te(^{37}Cl,5n) at a beam energy of 166 MeV. Details for each experiment are given separately in what follows.

2.1. First experiment

The target consisted of two stacked foils of 700 μg/cm^2 enriched to 99.29% of ^{130}Te, on a thin (~400 μg/cm^2) Au supporting foil. The Nordball spectrometer was equipped with 19 Compton suppressed HPGe detectors, one planar LEP detector and 39 of the 60 crystals of the BaF_2 ball. A total of more than 2×10^9 double and higher fold coincidence events were collected.

Energy-dependent gates were applied to the Ge time signals in order to exclude events caused by neutrons without degrading the efficiency for low energy gamma rays. Gates on the fold and sum-energy signals from the BaF_2 ball were imposed to enhance the 5n channel. With these conditions,[2] three γ–γ matrices and one γ–γ–γ cube were created:

(1) Coincidences between any two Ge detectors. This matrix was used to build the main part of the level scheme and to extract the gamma ray energies and relative intensities. The efficiency calibration of the set of Ge detectors was obtained from standard radioactive sources and checked in the low energy region by a calibration from

[2] The enhancement of the 5n channel was applied only in the first two matrices. In the other two cases wider gates were used to avoid degrading the statistics.

coincidence data. This calibration was produced by gating on transitions lying high up in the yrast band of ^{162}Er, which was also populated in the reaction.

(2) Coincidences between the LEP detector and any of the Ge detectors. The analysis of this matrix was useful to resolve transitions with very close energy appearing in coincidence with the same gates. Such situations occur often at low energy, where the LEP detector is efficient.

(3) Coincidences between the Ge detectors at angles of 37° or 143° with respect to the beam direction and the detectors at 79° or 101°, used for DCO analysis. When gating on a stretched quadrupole transition, the intensity ratio

$$\frac{I_\gamma(\text{observed at } 79^\circ \text{ or } 101^\circ, \text{ gate at } 37^\circ \text{ or } 143^\circ)}{I_\gamma(\text{observed at } 37^\circ \text{ or } 143^\circ, \text{ gate at } 79^\circ \text{ or } 101^\circ)}$$

should be ≈ 1.0 for a stretched quadrupole transition and ≈ 1.6 for a stretched dipole transition; note, however, that this latter value can be somewhat modified in practice by de-alignment of the nuclear spin and by non-zero mixing ratios. The information about the multipolarity of interband transitions resulting from this analysis has been essential to determine the spin and parity of the bands and for the subsequent configuration assignment.

(4) Triple coincidences between any of the Ge detectors. The analysis of this cube improved the level scheme obtained from the first matrix. It was particularly crucial for establishing interband transitions.

The data in all these matrices and cube were analysed using the programs ESCL8R, GF2 and LEVIT8R by D.C. Radford [2].

2.2. *Second experiment*

The ^{130}Te target had a thickness of 1 mg/cm^2 and was backed with 15 mg/cm^2 Au. The Nordball spectrometer consisted of 19 Compton suppressed HPGe detectors, the full 60 crystal element BaF_2 ball and one "clover" detector. A total of approximately 1×10^9 triple and higher fold coincidence events were collected. These data have been analysed in terms of lifetimes of the collective transitions in the quasi continuum in a separate work [3].

For the present work, energy-dependent time gates were imposed and higher fold events were decomposed into triples. This resulted in more than 500×10^6 Ge–Ge–Ge coincidence events, which were sorted into a γ–γ–γ cube. The analysis of the data in this cube, carried out with the program LEVIT8R by Radford [2], was of great use to improve the level scheme obtained from the matrices of the first experiment. This was particularly important for the determination of the weakest bands and many of the interconnecting transitions, as well as for solving the complicated decay pattern at the bottom of some bands.

Table 1
Gamma ray transitions assigned to ^{162}Tm

E_γ (keV)	I_γ	E_i (keV) [a]	E_f (keV) [a]	J_i^π	J_f^π	DCO
68.14(16)		305.2	237.8	9^-	8^-	
73.87(16)		237.8	163.8	8^-	6^-	
81.50(16)	≈30	233.0	151.5	7^+	6^+	
90.39(58)	16.7(14)	413.8	323.4	9^+	8^+	
95.88(16)	366.3(127)	401.1	305.2	10^-	9^-	
95.95(19)	≈10	233.0	137.0	7^+	6^+	
96.00(40)		203.1	108.1	7^+	6^+	
96.00(40)		96.4	0.0	6^+	5^+	
97		$x+97$	x	7^+	6^+	
98.86(31)	5.0(10)	413.8	314.9	9^+	8^+	
99.55(16)	141.6(81)	393.4	294.0	9^+	8^+	
102.60(48)	≈10	$x+200$	$x+97$	8^+	7^+	
103.40(40)		314.9	211.4	8^+	7^+	1.54(25)
103.60(40)		211.4	107.7	7^+	6^+	
105.49(48)	11.6(10)	556.0	450.2	10^+	9^+	
106.60(30)		203.1	96.4	7^+	6^+	
107.40(40)	≈10	107.7	0.0	6^+	5^+	
111.11(27)	33.5(18)	314.9	203.1	8^+	7^+	1.45(18)
111.93(16)	15.0(29)	323.4	211.4	8^+	7^+	
113.95(15)	442.4(141)	515.0	401.1	11^-	10^-	
114.98(22)	41.0(67)	211.4	96.4	7^+	6^+	
115.55(19)	50.1(31)	305.2	189.8	9^-	7^-	
120.30(30)		323.4	203.1	8^+	7^+	
126.32(17)	17.5(21)	$x+326$	$x+200$	9^+	8^+	
126.87(16)	33.6(14)	450.2	323.4	9^+	8^+	
131.29(16)		131.3	0.0	5^+	5^+	
131.35(19)	25.0(30)	$x+326$	$x+195$	9^+	8^+	
133.05(16)	129.9(58)	526.5	393.4	10^+	9^+	
133.12(20)	19.3(14)	729.1	596.0	11^+	10^+	
135.35(17)	30.2(14)	450.2	314.9	9^+	8^+	
142.28(27)		556.0	413.8	10^+	9^+	
145.48(16)	38.9(16)	596.0	450.2	10^+	9^+	
156.64(15)	503.2(155)	671.5	515.0	12^-	11^-	
160.55(17)	36.9(35)	393.4	233.0	9^+	7^+	
162.93(16)	7.0(30)	401.1	237.8	10^-	8^-	
163.50(30)		163.8	0.0	6^-	5^+	
164.00(16)	110.8(51)	690.5	526.5	11^+	10^+	
164.44(17)	33.7(35)	$x+490$	$x+326$	10^+	9^+	
167.55(15)	398.9(122)	839.0	671.5	13^-	12^-	
173	≈3	729.1	556.0	11^+	10^+	
182.22(17)	14.4(11)	596.0	413.8	10^+	9^+	
182.32(34)	4.5(10)	911.4	729.1	12^+	11^+	
183.88(17)	27.2(34)	$x+674$	$x+490$	11^+	10^+	
192.15(22)	35.6(53)	787.2	596.0	11^+	10^+	
192.28(22)	20.0(20)	979.5	787.2	12^+	11^+	
192.95(16)	68.3(34)	883.4	690.5	12^+	11^+	
193.23(18)	9.5(9)	567.0	373.2	8^-	6^-	
202.29(20)	22.9(17)	413.8	211.4	9^+	7^+	
207.26(18)	17.5(16)	314.9	108.1	8^+	6^+	
209.32(16)	66.3(24)	515.0	305.2	11^-	9^-	

Table 1 — continued

E_γ (keV)	I_γ	E_i (keV) [a]	E_f (keV) [a]	J_i^π	J_f^π	DCO
212.90(15)	364.6(111)	1051.9	839.0	14^-	13^-	
217.05(16)	39.5(24)	1100.5	883.4	13^+	12^+	
222.71(15)	274.3(83)	1274.6	1051.9	15^-	14^-	
225.83(17)	30.3(18)	$x+900$	$x+674$	12^+	11^+	
228		$x+326$	$x+97$	9^+	7^+	
232.03(17)	12.9(31)	1459.3	1227.3	14^+	13^+	
232.66(35)	10.3(9)	556.0	323.4	10^+	8^+	
232.68(16)	54.8(27)	526.5	294.0	10^+	8^+	
234.49(30)	2.8(6)	1375.5	1141.0	13^-	12^-	
236.53(18)	24.3(16)	$x+1137$	$x+900$	13^+	12^+	
239.80(40)		1150.7	911.4	13^+	12^+	
241.17(16)	71.8(26)	556.0	314.9	10^+	8^+	
243.80(16)	33.9(20)	1344.3	1100.5	14^+	13^+	
247.49(17)	16.1(8)	1227.3	979.5	13^+	12^+	
248.21(17)	12.2(8)	815.0	567.0	10^-	8^-	
256.21(15)	225.1(69)	1530.8	1274.6	16^-	15^-	
258.11(18)	10.4(18)	1999.7	1741.6	16^+	15^+	
260.95(17)	25.1(22)	1605.2	1344.3	15^+	14^+	
262.45(18)	14.5(12)	2536.3	2273.7	18^+	17^+	
263.03(28)	4.1(6)	1816.5	1553.9	15^-	14^-	
263.70(17)	18.6(16)	2800.0	2536.3	19^+	18^+	
270.28(16)	123.2(40)	671.5	401.1	12^-	10^-	
272.34(18)	16.7(53)	596.0	323.4	10^+	8^+	
274.00(18)	19.3(10)	2273.7	1999.7	17^+	16^+	
274.09(18)	21.3(14)	$x+1411$	$x+1137$	14^+	13^+	
276.26(17)	20.8(40)	3076.2	2800.0	20^+	19^+	
278.49(16)	156.8(48)	1809.7	1530.8	17^-	16^-	
280.21(20)	6.0(8)	2334.0	2053.8	17^-	16^-	
281.07(18)	16.3(11)	$x+1692$	$x+1411$	15^+	14^+	
282.27(17)	17.8(11)	1741.6	1459.3	15^+	14^+	
284.25(16)	29.8(26)	3360.5	3076.2	21^+	20^+	
285.54(18)	15.8(13)	1890.7	1605.2	16^+	15^+	
286.55(16)	129.7(40)	2096.3	1809.7	18^-	17^-	
290.57(28)	7.8(10)	$x+490$	$x+200$	10^+	8^+	
293.01(28)	5.3(11)	1010.6	717.9	11^-	9^-	
296	≈ 3	1664.4	1369.2	15^+	14^+	
297.10(16)	97.8(45)	690.5	393.4	11^+	9^+	
297.35(19)	14.6(27)	2188.0	1890.7	17^+	16^+	
301.75(16)	30.3(21)	3662.2	3360.5	22^+	21^+	
303.48(18)	5.1(12)	3821.5	3517.6	22^+	21^+	
306.34(16)	73.7(29)	2731.4	2425.0	20^-	19^-	
309.10(30)	12.9(13)	$x+2001$	$x+1692$	16^+	15^+	
312.41(17)	24.9(21)	3974.6	3662.2	23^+	22^+	
313.50(30)	10.6(11)	$x+2314$	$x+2001$	17^+	16^+	
314.72(24)	45.9(21)	729.1	413.8	11^+	9^+	
316.74(16)	49.2(19)	3418.6	3101.9	22^-	21^-	
319.40(18)	11.6(19)	2507.4	2188.0	18^+	17^+	
323.07(17)	30.6(16)	4140.3	3817.3	24^-	23^-	
323.79(16)	231.6(73)	839.0	515.0	13^-	11^-	
324.47(23)	13.1(26)	4146.5	3821.5	23^+	22^+	

Table 1 — continued

E_γ (keV)	I_γ	E_i (keV) [a]	E_f (keV) [a]	J_i^π	J_f^π	DCO
325.88(17)	25.4(20)	1141.0	815.0	12^-	10^-	
326.69(19)	10.7(15)	2834.1	2507.4	19^+	18^+	
328.37(16)	88.2(33)	2425.0	2096.3	19^-	18^-	
335.25(17)	22.2(19)	4309.9	3974.6	24^+	23^+	
335.48(19)	19.4(11)	4890.8	4554.9	26^-	25^-	
337.03(17)	26.7(27)	787.2	450.2	11^+	9^+	
344.62(18)	10.3(12)	4491.1	4146.5	24^+	23^+	
344.37(22)	6.8(9)	3178.9	2834.1	20^+	19^+	
345.61(17)	16.8(13)	4655.5	4309.9	25^+	24^+	
348.03(19)	17.8(18)	$x + 674$	$x + 326$	11^+	9^+	
355.20(16)	130.6(48)	911.4	556.0	12^+	10^+	
355.44(26)	4.7(11)	567.0	211.4	8^-	7^+	
356.95(16)	107.1(49)	883.4	526.5	12^+	10^+	
360.00(17)	13.2(10)	5684.9	5324.9	28^-	27^-	
364.17(19)	9.2(9)	4855.3	4491.1	25^+	24^+	
364.64(17)	12.7(11)	1375.5	1010.6	13^-	11^-	
370.26(17)	13.5(15)	5025.8	4655.5	26^+	25^+	
370.31(16)	56.0(22)	3101.9	2731.4	21^-	20^-	
380.17(16)	240.2(98)	1051.9	671.5	14^-	12^-	
380.43(18)	13.1(20)	5406.5	5025.8	27^+	26^+	
384.01(17)	28.7(14)	979.5	596.0	12^+	10^+	
388.38(34)	8.0(9)	6539.2	6150.8	30^-	29^-	
389.40(50)		2053.8	1664.4	16^-	15^+	
393.35(22)	6.0(9)	5642.7	5249.1	27^+	26^+	
393.89(24)	5.6(9)	5249.1	4855.3	26^+	25^+	
398.43(16)	40.8(19)	3817.3	3418.6	23^-	22^-	
401.48(18)	10.8(11)	5808.3	5406.5	28^+	27^+	
401.62(18)	8.4(8)	815.0	413.8	10^-	9^+	1.48(15)
403.03(34)	4.1(18)	717.9	314.9	9^-	8^+	
403.57(22)	5.3(14)	1553.9	1150.7	14^-	13^+	1.56(25)
409.81(20)	22.9(23)	$x + 900$	$x + 490$	12^+	10^+	
410.10(16)	100.5(43)	1100.5	690.5	13^+	11^+	
411.89(22)	6.8(8)	1141.0	729.1	12^-	11^+	
412.87(48)	4.6(11)	7458.6	7045.7	32^-	31^-	
412.96(18)	8.9(10)	6221.3	5808.3	29^+	28^+	
413.48(19)	30.4(25)	1553.9	1141.0	14^-	12^-	
414.62(16)	24.2(14)	4554.9	4140.3	25^-	24^-	
418.58(29)	3.8(10)	6061.2	5642.7	28^+	27^+	
419.79(20)	7.8(18)	2334.0	1914.2	17^-	16^+	1.56(32)
420.79(26)	3.8(10)	6482.0	6061.2	29^+	28^+	
421.35(16)	49.4(20)	1150.7	729.1	13^+	11^+	
427.35(45)	2.1(7)	8442.5	8015.0	34^-	33^-	
429.45(25)	5.5(18)	6650.8	6221.3	30^+	29^+	
430		9488.2	9058.3	36^-	35^-	
434.07(48)	15.5(12)	5324.9	4890.8	27^-	26^-	
436.03(15)	307.0(94)	1274.6	839.0	15^-	13^-	
439.36(17)	34.5(17)	1227.3	787.2	13^+	11^+	
440.73(19)	25.5(19)	1816.5	1375.5	15^-	13^-	
443.70(30)	5.2(10)	7094.8	6650.8	31^+	30^+	
447.26(19)	10.7(19)	1816.5	1369.2	15^-	14^+	1.40(29)

Table 1 — continued

E_γ (keV)	I_γ	E_i (keV) [a]	E_f (keV) [a]	J_i^π	J_f^π	DCO
454.55(21)	5.7(9)	1010.6	556.0	11^-	10^+	1.45(23)
458	≈4	7552.3	7094.8	32^+	31^+	
457.86(16)	120.2(45)	1369.2	911.4	14^+	12^+	
460.54(16)	113.1(46)	1344.3	883.4	14^+	12^+	
462.34(18)	27.2(17)	$x + 1137$	$x + 674$	13^+	11^+	
464.05(20)	9.6(19)	1375.5	911.4	13^-	12^+	1.53(25)
465.91(18)	9.1(10)	6150.8	5684.9	29^-	28^-	
479.70(16)	261.5(80)	1530.8	1051.9	16^-	14^-	
479.71(17)	33.9(18)	1459.3	979.5	14^+	12^+	
500.23(17)	34.7(12)	2053.8	1553.9	16^-	14^-	
504.45(16)	111.8(48)	1605.2	1100.5	15^+	13^+	
506.44(48)	5.5(9)	7045.7	6539.2	31^-	30^-	
510.48(18)	26.6(25)	$x + 1411$	$x + 900$	14^+	12^+	
513.87(17)	41.8(19)	1664.4	1150.7	15^+	13^+	
514.82(16)	51.0(20)	1741.6	1227.3	15^+	13^+	
517.26(18)	26.9(18)	2334.0	1816.5	17^-	15^-	
526.28(16)	48.1(24)	2800.0	2273.7	19^+	17^+	
532.17(17)	39.4(38)	2273.7	1741.6	17^+	15^-	
534.55(16)	271.1(86)	1809.7	1274.6	17^-	15^-	
536.51(18)	36.2(21)	2536.3	1999.7	18^+	16^+	
540.21(17)	38.6(58)	3076.2	2536.3	20^+	18^+	
540.49(18)	22.2(44)	1999.7	1459.3	16^+	14^+	
544		2800.0	2255.4	19^+	17^+	
545.07(16)	104.0(38)	1914.2	1369.2	16^+	14^+	
546.51(16)	95.3(42)	1890.7	1344.3	16^+	14^+	
552.06(17)	21.5(18)	3076.2	2524.2	20^+	18^+	1.04(10)
555.84(18)	29.8(20)	$x + 1692$	$x + 1137$	15^+	13^+	
556.37(48)	4.0(10)	8015.0	7458.6	33^-	32^-	
560.37(16)	64.3(28)	3360.5	2800.0	21^+	19^+	
565.12(16)	252.5(78)	2096.3	1530.8	18^-	16^-	
582.14(18)	22.4(10)	2636.0	2053.8	18^-	16^-	
583.08(16)	98.1(41)	2188.0	1605.2	17^+	15^+	
586.14(16)	65.4(55)	3662.2	3076.2	22^-	20^+	
590.14(17)	26.1(16)	2923.7	2334.0	19^-	17^-	
590.48(19)	21.9(20)	$x + 2001$	$x + 1411$	16^+	14^+	
591.32(17)	33.8(18)	2255.4	1664.4	17^+	15^+	
605.42(19)	12.5(8)	4146.5	3540.8	23^+	21^+	1.13(11)
609.35(24)	6.0(10)	2273.7	1664.4	17^+	15^+	
610.36(16)	66.6(26)	2524.2	1914.2	18^+	16^+	
614.27(17)	58.2(22)	3974.6	3360.5	23^+	21^+	
615.72(16)	203.6(68)	2425.0	1809.7	19^-	17^-	
616.87(16)	76.3(25)	2507.4	1890.7	18^+	16^+	
622.08(17)	28.8(20)	2536.3	1914.2	18^+	16^+	1.00(12)
622.45(20)	21.5(17)	$x + 2314$	$x + 1692$	17^+	15^-	
628.06(19)	16.1(24)	4146.5	3517.6	23^+	21^+	
631.70(18)	10.1(11)	4510.4	3878.7	24^-	22^-	
634.47(36)	5.5(10)	3270.5	2636.0	20^-	18^-	
635.09(16)	200.6(62)	2731.4	2096.3	20^-	18^-	
646.21(16)	85.7(35)	2834.1	2188.0	19^+	17^+	
647.38(17)	59.3(20)	4309.9	3662.2	24^+	22^+	

Table 1 — continued

E_γ (keV)	I_γ	E_i (keV) [a]	E_f (keV) [a]	J_i^π	J_f^π	DCO
649.50(34)	12.4(13)	$x+2651$	$x+2001$	18^+	16^+	
651.20(23)	10.7(12)	$x+2965$	$x+2314$	19^+	17^+	
654.36(18)	26.4(14)	2910.1	2255.4	19^+	17^+	
658.50(55)	21.2(16)	3183.7	2524.2	20^+	18^+	
658.50(55)	10.0(10)	4519.9	3861.8	24^+	22^+	
659.68(18)	24.4(15)	3583.4	2923.7	21^-	19^-	
661.51(20)	12.5(7)	3297.5	2636.0	20^-	18^-	
669.93(22)	14.9(21)	4491.1	3821.5	24^+	22^+	
670.91(17)	63.7(28)	3178.9	2507.4	20^+	18^+	
671.30(17)	8.1(9)	4868.1	4196.5	25^-	23^-	
677.06(16)	144.3(47)	3101.9	2425.0	21^-	19^-	
678.34(18)	15.4(13)	3861.8	3183.7	22^+	20^+	
681.20(17)	52.9(20)	4655.5	3974.6	25^+	23^+	
683.44(17)	31.0(23)	3517.6	2834.1	21^+	19^+	0.97(8)
687.37(16)	152.8(48)	3418.6	2731.4	22^-	20^-	
699.60(18)	16.1(9)	3609.4	2910.1	21^+	19^+	
703.39(18)	13.9(18)	2800.0	2096.3	19^+	18^-	1.33(13)
705.71(19)	13.5(10)	5215.5	4510.4	26^-	24^-	
706.35(17)	29.4(19)	3540.8	2834.1	21^+	19^+	
709.21(22)	15.5(23)	4855.3	4146.5	25^+	23^+	
710.64(28)	6.1(5)	4008.2	3297.5	22^-	20^-	
711.72(17)	42.8(18)	3890.0	3178.9	22^+	20^+	
714.70(50)	3.5(8)	5234.1	4519.9	26^+	24^+	
715.60(16)	111.6(39)	3817.3	3101.9	23^-	21^-	
716.86(17)	39.7(16)	5025.8	4309.9	26^+	24^+	
718.71(23)	10.7(9)	4259.6	3540.8	23^+	21^+	
721.25(16)	106.8(39)	4140.3	3418.6	24^-	22^-	
722.93(19)	18.1(13)	4613.0	3890.0	24^+	22^+	
725.08(20)	14.1(18)	1999.7	1274.6	16^+	15^-	1.43(35) [b]
725.16(19)	15.2(13)	4308.7	3583.4	23^-	21^-	
726.56(29)	13.3(19)	2536.3	1809.7	18^+	17^-	1.43(35) [b]
729.58(28)	5.3(11)	5249.1	4519.9	26^+	24^+	
731.01(23)	9.0(9)	4340.5	3609.4	23^+	21^+	
734.52(18)	13.3(10)	5602.7	4868.1	27^-	25^-	
737.53(16)	64.6(25)	4554.9	3817.3	25^-	23^-	
742.07(33)	5.6(12)	4259.6	3517.6	23^+	21^+	0.99(15)
742.42(20)	12.5(18)	2273.7	1530.8	17^+	16^-	1.44(18)
742.50(40)	3.3(8)	5234.1	4491.1	26^+	24^+	
744.18(41)	3.4(4)	4752.2	4008.2	24^-	22^-	
750.45(16)	74.6(29)	4890.8	4140.3	26^-	24^-	
750.92(17)	40.9(26)	5406.5	4655.5	27^+	25^+	
754.05(20)	10.3(13)	5013.7	4259.6	25^+	23^+	
756.61(18)	12.7(13)	5369.6	4613.0	26^+	24^+	
758.65(25)	11.1(11)	5249.1	4491.1	26^+	24^+	
759.94(21)	6.4(9)	5100.5	4340.5	25^+	23^+	
761.12(17)	16.8(11)	5976.6	5215.5	28^-	26^-	
769.97(16)	42.6(19)	5324.9	4554.9	27^-	25^-	
776.83(20)	12.7(10)	5085.5	4308.7	25^-	23^-	
782.20(17)	35.4(24)	5808.3	5025.8	28^+	26^+	
786.89(21)	13.6(14)	5642.7	4855.3	27^+	25^+	

Table 1 — continued

E_γ (keV)	I_γ	E_i (keV) [a]	E_f (keV) [a]	J_i^π	J_f^π	DCO
792.24(18)	16.1(11)	6395.0	5602.7	29^-	27^-	
794.50(16)	50.9(21)	5684.9	4890.8	28^-	26^-	
798.94(22)	7.7(11)	5812.7	5013.7	27^+	25^+	
811.74(28)	9.6(14)	6061.2	5249.1	28^+	26^+	
814.84(17)	34.4(16)	6221.3	5406.5	29^+	27^+	
818.34(20)	9.3(12)	6187.8	5369.6	28^+	26^+	
819.68(23)	9.0(9)	5905.2	5085.5	27^-	25^-	
822.65(18)	14.3(10)	6799.3	5976.6	30^-	28^-	
826.00(17)	27.4(14)	6150.8	5324.9	29^-	27^-	
839.57(23)	9.9(12)	6482.0	5642.7	29^+	27^+	
842.63(17)	25.0(26)	6650.8	5808.3	30^+	28^+	
846.09(23)	6.2(13)	6658.7	5812.7	29^+	27^+	
847.82(20)	6.2(10)	6753.0	5905.2	29^-	27^-	
853.82(16)	39.0(18)	6539.2	5684.9	30^-	28^-	
861.20(17)	13.4(10)	7256.2	6395.0	31^-	29^-	
869.93(27)	5.4(12)	7528.7	6658.7	31^+	29^+	
873.24(18)	25.0(14)	7094.8	6221.3	31^+	29^+	
881.01(23)	6.1(12)	7069.0	6187.8	30^+	28^+	
889.40(47)	3.3(10)	8418.1	7528.7	33^+	31^+	
889.87(43)	6.7(12)	7371.5	6482.0	31^+	29^+	
894.96(17)	18.0(14)	7045.7	6150.8	31^-	29^-	
895.49(19)	10.4(11)	7694.7	6799.3	32^-	30^-	
901.16(18)	20.7(19)	7552.3	6650.8	32^+	30^+	
919.48(18)	25.1(15)	7458.6	6539.2	32^-	30^-	
929.17(20)	14.4(12)	8024.1	7094.8	33^+	31^+	
938.10(19)	9.2(9)	8194.3	7256.2	33^-	31^-	
939.54(22)	4.0(10)	8008.5	7069.0	32^+	30^+	
961.08(19)	15.5(17)	8513.0	7552.3	34^+	32^+	
969.57(19)	13.5(11)	8015.0	7045.7	33^-	31^-	
970.32(22)	7.6(9)	8665.3	7694.7	34^-	32^-	
984.01(21)	16.2(13)	8442.5	7458.6	34^-	32^-	
984.36(23)	9.1(10)	9008.6	8024.1	35^+	33^+	
1014.98(20)	6.3(8)	9209.3	8194.3	35^-	33^-	
1021.33(22)	8.7(10)	9534.5	8513.0	36^+	34^+	
1038.34(25)	6.9(9)	10046.3	9008.6	37^+	35^+	
1038.98(24)	4.9(8)	9704.3	8665.3	36^-	34^-	
1042.74(24)	10.1(9)	9058.3	8015.0	35^-	33^-	
1045.60(50)	8.0(9)	9488.2	8442.5	36^-	34^-	
1047.50(30)	≈ 4	5602.7	4554.9	27^-	25^-	
1050.48(22)	6.5(8)	4868.1	3817.3	25^-	23^-	0.95(16)
1075.60(21)	5.1(8)	5215.5	4140.3	26^-	24^-	
1082.05(27)	6.0(8)	10616.8	9534.5	38^+	36^+	
1089.64(29)	4.5(8)	10298.9	9209.3	37^-	35^-	
1090.21(31)	4.6(8)	11136.5	10046.3	39^+	37^+	
1091.80(21)	9.4(10)	4510.4	3418.6	24^-	22^-	0.91(13)
1094.66(23)	5.1(9)	4196.5	3101.9	23^-	21^-	0.92(15)
1104.20(50)	5.7(9)	10592.3	9488.2	38^-	36^-	
1113.00(48)	7.7(8)	10171.1	9058.3	37^-	35^-	
1138.16(38)	≈ 3	12274.5	11136.5	41^+	39^+	
1139.28(35)	4.1(7)	11756.1	10616.8	40^+	38^+	

Table 1 — continued

E_γ (keV)	I_γ	E_i (keV) [a]	E_f (keV) [a]	J_i^π	J_f^π	DCO
1147.35(19)	5.0(9)	3878.7	2731.4	22^-	20^-	0.90(33)
1152.20(50)	6.0(14) [c]	11744.6	10592.3	40^-	38^-	
1152.20(50)	6.0(14) [c]	12896.7	11744.6	42^-	40^-	
1175.00(48)	8.6(9)	11346.5	10171.1	39^-	37^-	
1176.53(43)	≈ 2	13451.6	12274.5	43^+	41^+	
1179.39(48)	≈ 2	12935.6	11756.1	42^+	40^+	
1194		14129.1	12935.6	44^+	42^+	
1198.88(40)	≈ 1	14650.3	13451.6	45^+	43^+	
1215		15865.3	14650.3	47^+	45^+	
1230.00(48)	6.1(9)	12576.0	11346.5	41^-	39^-	

[a] Excitation energies relative to the 24 ms, 5^+ isomer except for bands lA, kA, where they are given relative to the 6^+ state in lA. The unknown energy of this 6^+ state is called x.
[b] DCO ratio for sum of 725.08 and 726.56 keV transitions.
[c] Added intensities of both 1152.20 keV transitions.

3. Experimental results. Level scheme

The nucleus ^{162}Tm had been studied earlier using the (^{14}N,4n) [4] and the (^{37}Cl,5n) reactions [5]. From these studies two strongly and one weakly coupled bands were established to maximum spins of 22–26 $\hbar$. The results of the present work represent a significant extension of the former. The gamma rays assigned to ^{162}Tm are listed in Table 1, with their corresponding energy, intensity, spin and parity data. DCO ratios are also given for selected transitions. The level scheme and representative spectra are shown in Figs. 1 and 2, respectively. The bands are labelled by the appropriate Nilsson labels, as well as by a combination of lower and upper case letters which indicate the quasiparticle configurations for the odd proton and neutron, respectively, at low spin. The meaning and justification of these labels are given in the next section and in Table 2.

The bands previously known are (fA,eA), (bA,aA) and (dA,cA). They have been extended to higher spins and, in some cases, changes have been introduced in the low spin part with respect to the results of Refs. [4,5]. In addition, we have found five new bands, corresponding to four coupled bands with M1 transitions connecting signature partners and one weakly coupled band. Apart from a non-observed low energy transition in one of the new structures ($6^+ \to 5^+$ in lA, kA), all the bands are interconnected. Thus the excitation energy of all the states except those of lA, kA above its 5^+ band head is determined. Many of the connecting transitions are due to mixing at band crossings; examples are found at both low and higher spin values, the maximum being $I = 26\hbar$ (fE crossing with dA).

The highest spin, $I = 47\hbar$, is established in one of the new structures, fH. (See the two upper panels of Fig. 2a.) This is most likely related to the fact that above $I \simeq 33\hbar$ this sequence becomes yrast, as demonstrated in Fig. 3. The upper part of the bands has

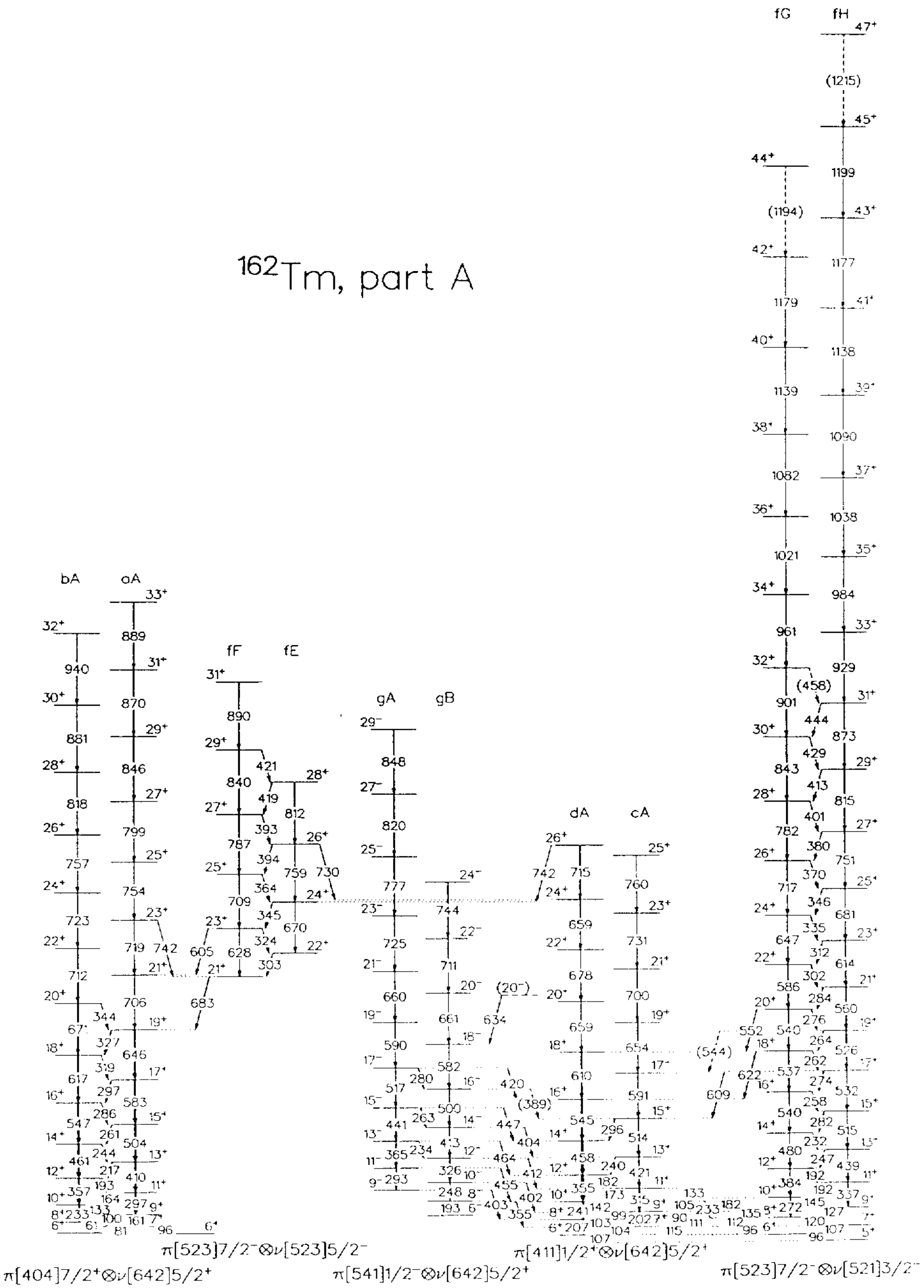

Fig. 1. Level scheme of ^{162}Tm divided into parts A and B.

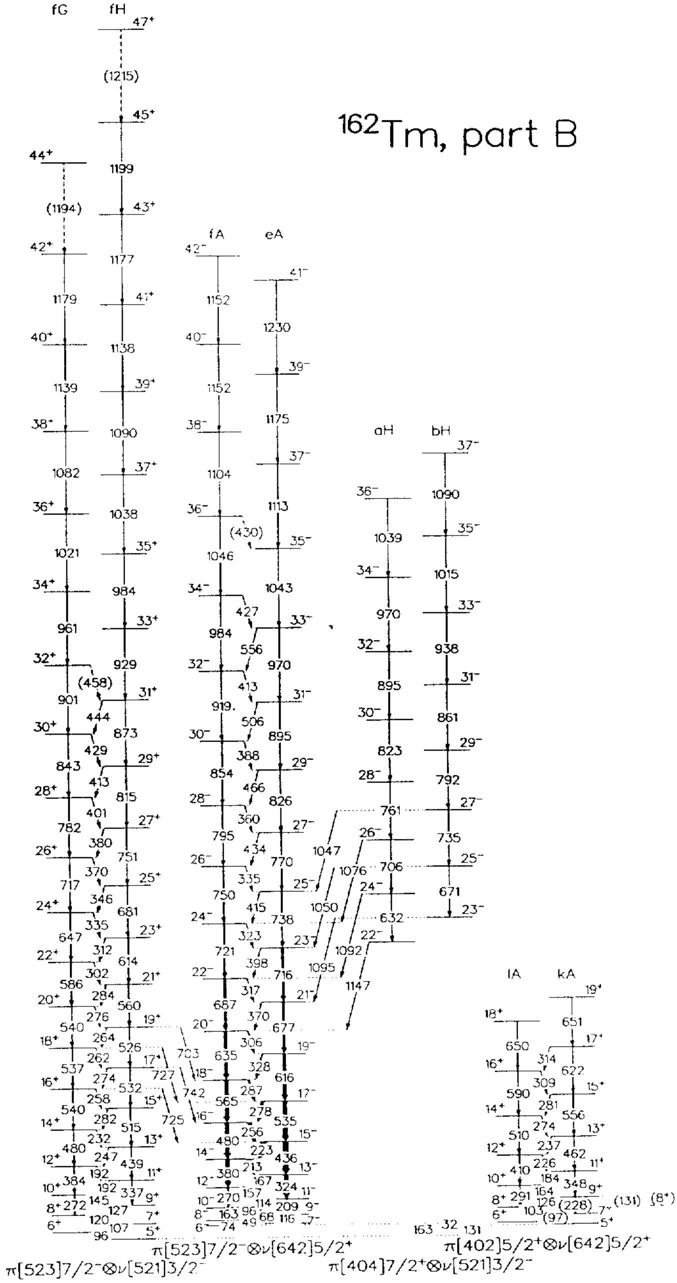

Fig. 1 — continued.

been obtained exclusively from the γ–γ data of the first experiment, since the backed target of the second experiment gives rise to very broad peaks in this region. The low spin part at the bottom of the bands is established in most cases. The γ–γ–γ data from the second experiment has been crucial to determine the decay pattern in this region.

For coupled bands with connecting $\Delta I = 1$ M1 or mixed M1/E2 transitions the experimental values of $B(\mathrm{M1})/B(\mathrm{E2})$ have been extracted from the expression

$$B(\mathrm{M1})/B(\mathrm{E2}) = 0.697 \frac{T_{\gamma_1}}{T_{\gamma_2}} \frac{E_{\gamma_2}^5}{E_{\gamma_1}^3} \frac{1}{1+\delta^2}, \tag{1}$$

where γ_1 and γ_2 refer to the $\Delta I = 1$ and $\Delta I = 2$ transitions, respectively, with E_γ in MeV, and $\delta^2 = T_{\gamma_1}(\mathrm{E2})/T_{\gamma_1}(\mathrm{M1})$. The influence from the mixing ratio δ can be

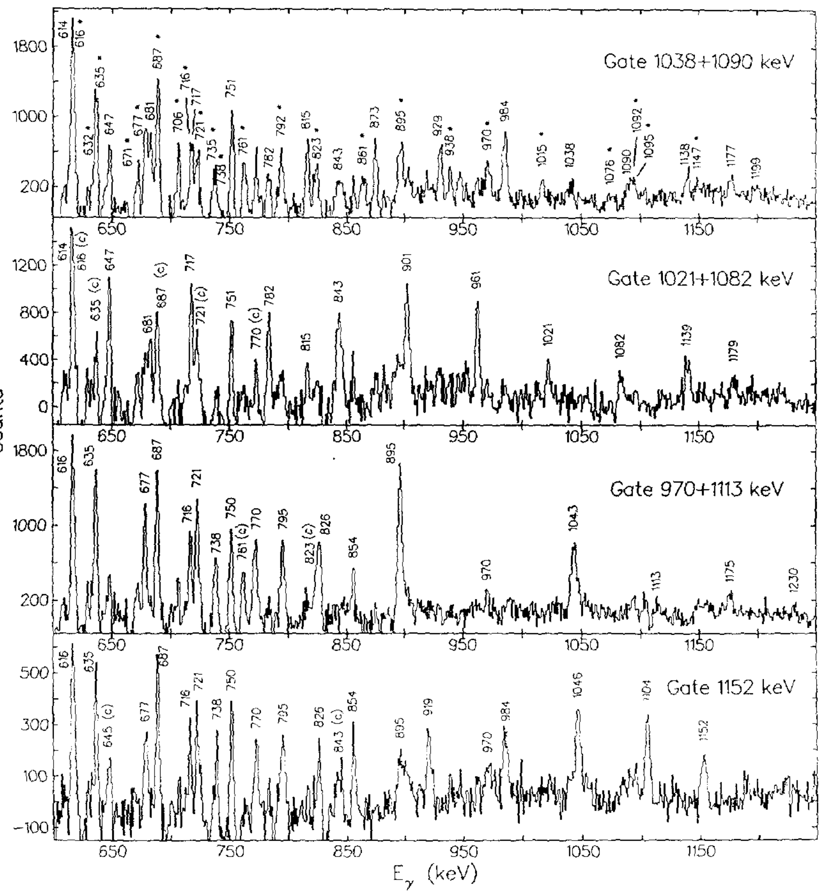

Fig. 2. Spectra documenting bands and connections. The vertical numbers are the peak energies in keV. Transitions marked with a (c) are contaminants. (a) Gated spectra from the γ–γ matrix. Gate 1038+1090 keV: bands fH, fG (note, in particular, the highest transitions of fH) and, marked with asterisks, aH, bH and their decay to fA, eA. Gate 1021+1082 keV: bands fG, fH (note the highest transitions of fG). Gate 970+1113 keV: bands eA, fA (note the highest transitions of eA). The contaminants marked and some excessively high peaks are due to the 970 keV transition in aH. Gate 1152 keV: bands fA, eA (note the highest transitions of fA).

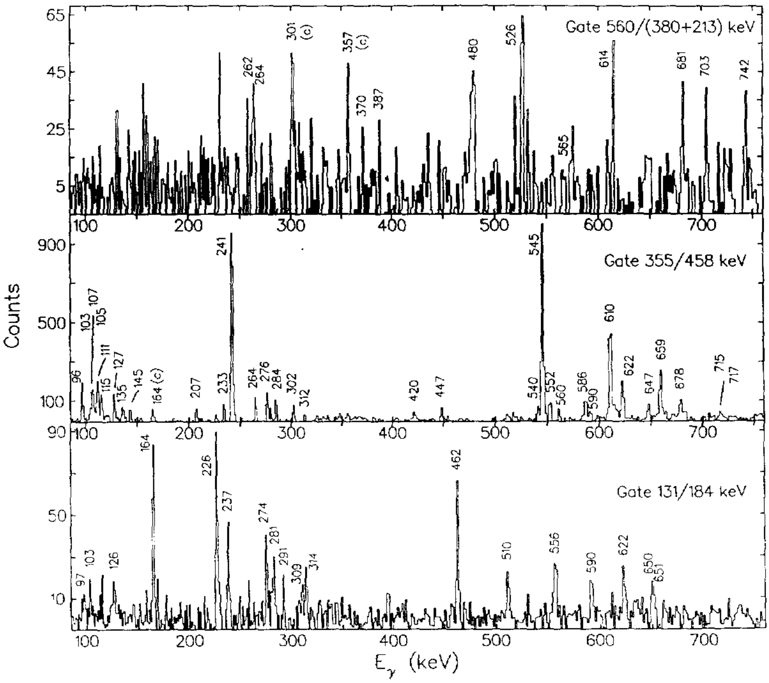

Fig. 2. (b) Doubly gated spectra from the γ-γ-γ cube. Gate 560/(380+213) keV: connections between bands fH and fA. Gate 355/458 keV: band dA and its connections with fG and gA. Gate 131/184 keV: bands lA, kA. Note that the gate at 131 keV corresponds to the suggested transition from kA to the 5^+ isomer, band head of fH (see discussion in Section 4).

Table 2

Band labels, configurations assigned, K-couplings and alignments. The K values and alignments are given in units of $\hbar$. Favoured K values predicted by the Gallagher–Moszkowski (GM) rules are shown next to the assigned ones. All alignments are at $\hbar\omega$ = 0.2 MeV and with Harris parameters $\mathcal{J}_0 = 30\,\hbar^2$/MeV and $\mathcal{J}_1 = 40\,\hbar^4/\text{MeV}^3$. The two columns under "i_x (exper.)" are the experimental alignments for bands in ^{162}Tm. Those under "i_x (added)" are the sums of the proton and neutron components, extracted from the averages for ^{161}Tm, ^{163}Tm and for ^{161}Er, ^{163}Yb respectively

Labels		Nilsson configuration	K^π	K_{favoured}	i_x (exper.)		i_x (added)	
$\alpha = 0$	$\alpha = 1$	at low spin	(ass.)	(GM)	$\alpha = 0$	$\alpha = 1$	$\alpha = 0$	$\alpha = 1$
bA	aA	$\pi[404]7/2^+ \otimes \nu[642]5/2^+$	6^+	1	5.5	5.5	5.4	5.4
dA	cA	$\pi[411]1/2^+ \otimes \nu[642]5/2^+$	2^+	2	6.0	5.7	6.0 [a]	5.8 [a]
lA	kA	$\pi[402]5/2^+ \otimes \nu[642]5/2^+$	5^+	5	4.7	4.7	5.4 [a]	5.0 [a]
fA	eA	$\pi[523]7/2^- \otimes \nu[642]5/2^+$	6^-	6	7.0	6.9	7.1	6.9
gB	gA	$\pi[541]1/2^- \otimes \nu[642]5/2^+$	2^-	2	6.8	7.1	6.7	8.2
fE	fF	$\pi[523]7/2^- \otimes \nu[523]5/2^-$	6^+	1				
fG	fH	$\pi[523]7/2^- \otimes \nu[521]3/2^-$	5^+	5	5.2	5.1	4.9	4.5 [b]
aH	bH	$\pi[404]7/2^+ \otimes \nu[521]3/2^-$	5^-	2				

[a] Only ^{163}Tm used for the proton component (no ^{161}Tm data available for this configuration).
[b] Only ^{161}Er used for the neutron component (no ^{163}Yb data available for this configuration).

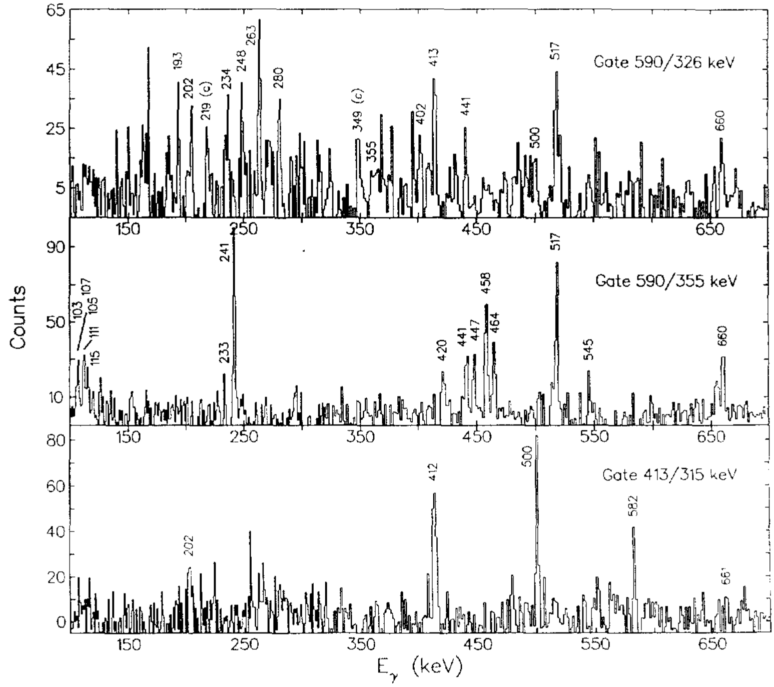

Fig. 2. (c) Doubly gated spectra from the γ-γ-γ cube. Gate 590/326 keV: connections between bands gA and gB. Gate 590/355 keV: connections between bands gA and dA. Gate 413/315 keV: connection between bands gB and cA.

estimated from the results of rigid rotation calculations [6]. The correction is in general less than 10% and has therefore been neglected.

4. Spin and parity determination

In none of the previous investigations [4,5] of ^{162}Tm were spin and parity deduced in a model-independent way, and the relative excitation energy of the different bands was not determined either. In the present work the observed interband transitions fix the relative energies of all the bands, except lA, kA (see Fig. 1). DCO ratios have been extracted for many of these transitions (see Table 1), providing information about their multipolarity which makes it possible to assign spin and often parity of levels in a model-independent way (also with the exception of lA, kA). These assignments are presented for the individual bands below.

4.1. Bands fG, fH

These bands are connected to fA, eA and to dA, cA with several transitions (see the upper and mid panel of Fig. 2b). The bottom of band fH is found to coincide with the 24 s isomeric 5^+ state [7]. Furthermore, the assignment of the structure of this band

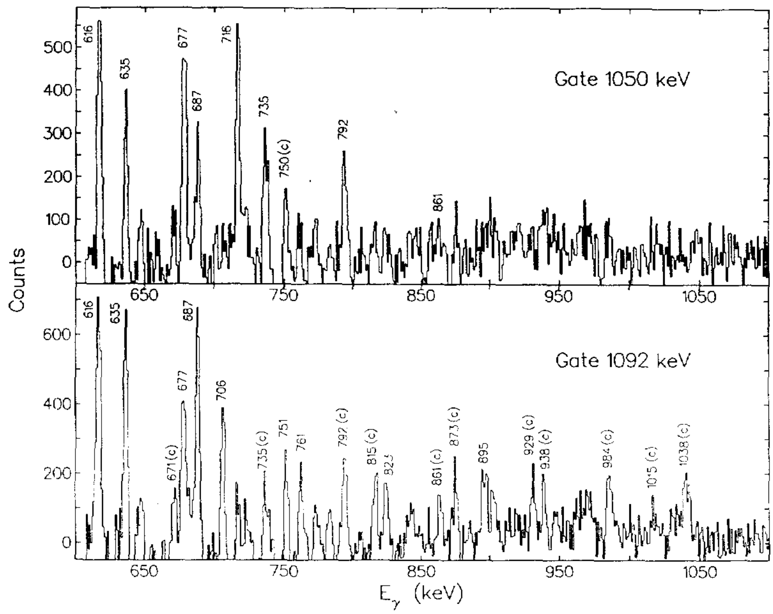

Fig. 2. (d) Gated spectra from the γ-γ matrix. Gate 1050 keV: decay of band bH to eA. Gate 1092 keV: decay of band aH to fA. The contaminants marked are due to the 1090 keV transition in fH and to the 1090 and 1095 keV transitions in bH.

is in agreement with the suggestion of Ref. [4] for that of the 5^+ isomeric state (see Section 5.2). This band can therefore be used as a firm basis to which all other bands are related.

4.2. Bands fA, eA

The yrast band, fA, eA, known before [4,5] up to $I = 26, 25\hbar$, has been extended to $I = 42, 41\hbar$ (see the 2 lower panels of Fig. 2a). The decay of the lowest state (6^-) of band fA by a 163 keV transition to the known 24 s isomeric 5^+ state (band head of fH, see above) is confirmed. The spin assignments of Ref. [4] are based on a good agreement with expectations concerning alignment and values of $B(\mathrm{M1})/B(\mathrm{E2})$ for the configuration $\pi[523]7/2^- \otimes \nu[642]5/2^+$, which is built on the lowest orbits in the odd proton and neutron neighbours. The DCO ratios obtained in the present work for the transitions of 703, 742 keV (fH → fA) and 727, 725 keV (fG → eA) are consistent with stretched dipoles. This enables us to confirm the spin and parity assignments for levels in bands fA, eA [4] in a model-independent way.

4.3. Bands dA, cA

These bands were known before [5] to the levels marked with spins 20,21 $\hbar$, but assigned one spin unit higher in [5]. The bottom of these bands are in the present

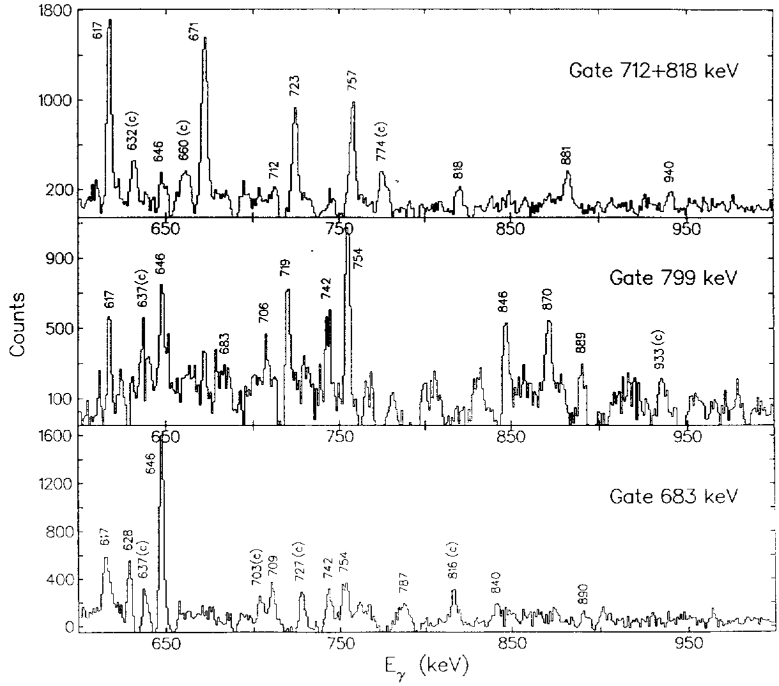

Fig. 2. (e) Gated spectra from the γ-γ matrix. Gate 712+818 keV: bands bA, aA (note the highest transitions of bA). Gate 799 keV: bands aA, bA (note the highest transitions of aA). Gate 683 keV: connection between bands aA and fF.

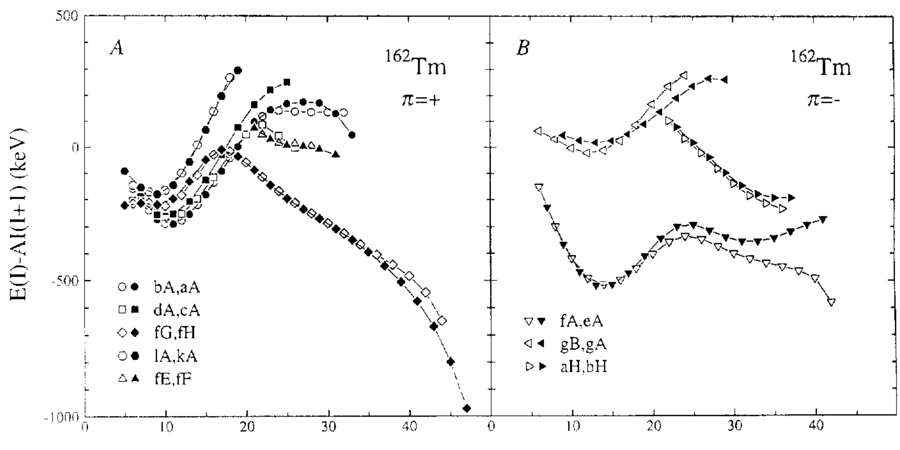

Fig. 3. Energy versus spin for positive and negative parity bands in ^{162}Tm relative to a rigid reference with a moment of inertia of $\mathcal{J} = 67\hbar^2$ MeV^{-1}.

experiment changed and further developed. The bands dA, cA are connected to bands fG, fH in the spin range 15–18 $\hbar$, by transitions of energies very close to the in-band E2 transitions (see the mid panel of Fig. 2b). The structure of the bands and connecting transitions is a clear signature of an accidental crossing, with the closest levels at $I = 17, 18\hbar$. This interpretation is consistent with stretched quadrupole character from the DCO ratios for these connecting transitions. Therefore, spin and parity for bands dA, cA are firmly determined. Besides the change in spin assignment mentioned above, the positive parity is opposite to Ref. [5]. Close to the levels with $I = 7, 8\hbar$, the two band structures come very close again and many cross band transitions are observed, which are fully consistent with our assignments for dA, cA.

4.4. Bands gA, gB

Several transitions exist between bands gA, gB and dA, cA with energies around 400 keV (see Fig. 2c). The DCO ratios obtained for the strongest of these transitions are consistent with stretched dipole character. This firmly determines spins for levels in bands gA, gB. If these stretched dipole transitions were of M1 character, they would represent a very unusual decay pattern of interband transitions with large reduced M1 matrix elements, whereas E1 transitions competing with in-band transitions are observed both in odd proton and odd neutron nuclei between certain configurations (see Sections 5.1.1 and 6.4). The bands gA, gB have therefore been assigned negative parity.

4.5. Bands aH, bH

These bands are connected to fA, eA by several transitions with energies around 1100 keV (see Fig. 2d). The corresponding DCO ratios, which could be determined for most of them, are consistent with stretched quadrupole character. The alternative option allowed by the DCO ratios are $I \rightarrow I$ quadrupole transitions. But these would imply that the band at $I \sim 30\hbar$ would have an excitation energy of $\sim$ 1 MeV, over band fA, eA, which would be in strong disagreement with the measured relative population intensity. (See Table 1 and Fig. 3.) Therefore, the spin and parity of aH, bH are rather firmly established.

4.6. Bands fE, fF

Band fE is connected to dA due to a crossing at $I = 26\hbar$, with two transitions of 730 keV (fE $\rightarrow$ dA) and 742 keV (dA $\rightarrow$ fE) of stretched quadrupole character. Spin and parity are therefore locked to those of band dA.

4.7. Bands bA, aA

These bands were established in Ref. [5] to $I = 22, 23\hbar$. In the present work they are confirmed in the range $8 < I < 19\hbar$ (see the upper and mid panel of Fig. 2e), but the structure is changed both below $I = 8\hbar$ and above $I = 19\hbar$. At the bottom, several gamma rays are re-ordered and added. At $I = 21, 23\hbar$, band aA is connected to fF due to a crossing (see the lower panel of Fig. 2e). From the DCO ratios, the stretched quadrupole character of the connecting transitions is confirmed, and therefore levels in these bands also have firm spin and parity assignment.

4.8. Bands lA, kA

All transitions in the bands lA, kA are in coincidence with a 131 keV transition (see the lower panel of Fig. 2b). This transition coincides in energy (within 0.16 keV) with the strongest branch from the 6^- band head of fA, which proceeds via an unobserved 32 keV transition [4] parallel to the direct 163 keV transition to the 5^+ band head of fH. On this basis the 131 keV transition is assigned as a connection between the 5^+ band heads of the bands kA and fH. Unfortunately, no DCO ratio could be determined for the 131 keV transition. This scenario implies a missing $7^+ \rightarrow 5^+$ transition at the bottom of band kA as well as a missing cross band transition between the 6^+ and 5^+ states of lA and kA, which would have to be coinciding with X-ray energies, or have an energy lower than ~ 35 keV, which is the limit implied by absorption in the target chamber. Such a low transition energy would not be inconsistent with the band structure of lA, kA close to the band head.

5. Identification of configurations

The bands expected at the lowest excitation energy are those built on the lowest quasiprotons and quasineutrons in the neighbouring odd-Z and odd-N nuclei. In ^{161,163}Tm [8,9] the lowest quasi-protons of positive and negative parity in the spin range 15–30$\hbar$ are built on the Nilsson configurations $g_{7/2}[404]7/2^+$ and $h_{11/2}[523]7/2^-$, respectively. At higher excitation energy bands built on the configurations $d_{3/2}[411]1/2^+$, $d_{5/2}[402]5/2^+$ and $h_{9/2}[541]1/2^-$ are also found. In the neighbouring odd neutron nuclei like ^{161}Er [10] and ^{163}Yb [11] the lowest positive parity band is based on the $i_{13/2}[642]5/2^+$ configuration, whereas two negative parity configurations, namely $f_{7/2}[521]3/2^-$ and $h_{9/2}[523]5/2^-$, are quite close in energy, the former being ground state in both nuclei. The 2-quasiparticle configurations that are assigned to the 8 bands studied in the present experiment are indeed composed of these lowest orbits as can be seen from Table 2. This table also shows for the coupled quasiparticle bands the favoured values of K according to the Gallagher–Moskowski rule [12] as well as expected summed alignments.

The rotational bands of Fig. 1 are shown in Fig. 3 as excitation energy versus spin relative to a rigid reference with a moment of inertia of 67 $\hbar^2$ MeV^{-1}. Alignment plots using a reference with Harris parameters $\mathcal{J}_0 = 35\hbar^2$ MeV^{-1} and $\mathcal{J}_1 = 40\hbar^4$ MeV^{-3} are shown in Fig. 4. Bands with positive and negative parity are separated in the two figures. In the interpretation of these bands in terms of constituent quasiprotons and

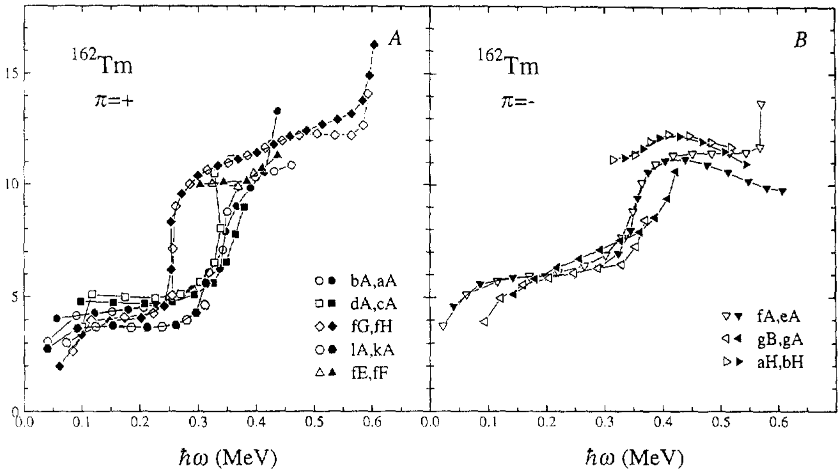

Fig. 4. Alignment versus rotational frequency for positive and negative parity bands in ^{162}Tm relative to a reference with Harris parameters $\mathcal{J}_0 = 35\hbar^2\text{MeV}^{-1}$ and $\mathcal{J}_1 = 40\hbar^4\text{MeV}^{-3}$

quasineutrons the relative excitation energy, alignments, crossing frequencies as well as $B(\text{M1})/B(\text{E2})$ values in the coupled bands, shown in Fig. 5, are utilized.

The calculated values of $B(\text{M1})/B(\text{E2})$, also shown in Fig. 5, are based on an extension of the geometrical model of Ref. [13]:

$$B(\text{M1}, I \to I-1) = \frac{3}{8\pi I^2}\left\{\sqrt{I^2-K^2}\left[\sum_j (g_j - g_R)\Omega_j\right] - K\left[\sum_j (g_j - g_R)\, i_j\right]\right\}^2 \mu_N^2. \tag{2}$$

The value used for the collective gyromagnetic ratio is $g_R = 0.35$. The parameter values for the individual constituents, g_j, Ω_j and alignment, i_j, are: For neutrons: A[3]: −0.26, 1.5, 4.5; E, F: 0.39, 2.5, 1.5; G, H: −0.61, 1.5, 1.5; for protons: a, b: 0.63, 3.5, 0; e, f: 1.29, 3.5, 1.0; k, l: 1.57, 2.5, 0, and for an aligned pair of $i_{13/2}$ quasineutrons a summed alignment of 6 and 9 $\hbar$ have been used for (BC) and (AB) respectively, together with $\Omega_j = 0$.

The values of $B(\text{E2}; I \to I-2)$ are calculated according to the expression [6]

$$B(\text{E2}, I \to I-2) = \frac{5}{16\pi} Q_0^2 \langle IK20|I-2K\rangle^2. \tag{3}$$

For all the bands in ^{162}Tm we have used $Q_0 = 6.5b$, which corresponds to an average of the experimental values for the neighbouring even–even Er and Yb nuclei [14].

The clearest distinction between the bands is connected to the lowest observed crossing frequency. Bands containing the $\nu i_{13/2}[642]5/2^+$ orbit have the normal $i_{13/2}$ (AB)

[3] In this case of a strongly alignable quasineutron we have used a reduced $\Omega_j = 1.5$ instead of 2.5.

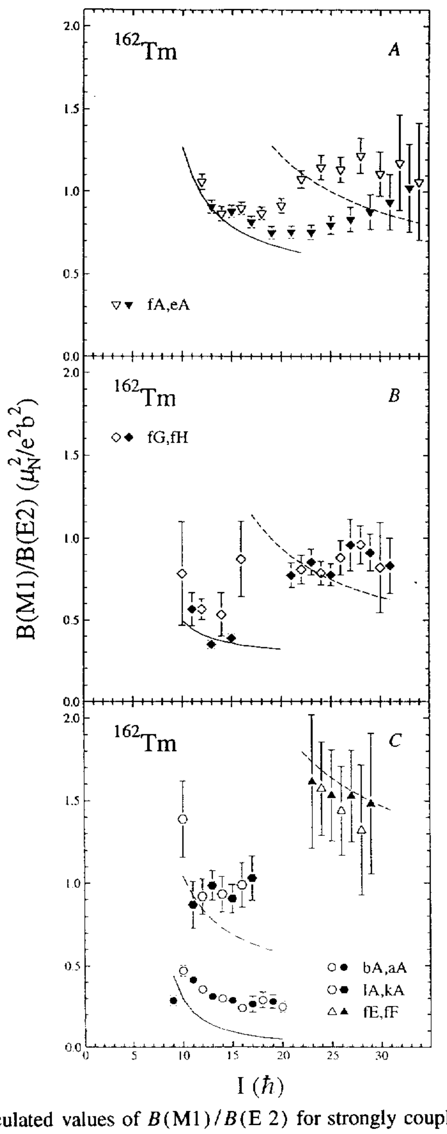

Fig. 5. Experimental and calculated values of $B(\mathrm{M1})/B(\mathrm{E2})$ for strongly coupled bands in ^{162}Tm. (a) Band $\pi h_{11/2}[523]7/2^- \otimes \nu i_{13/2}[642]5/2^+$, fA, eA. The curves corresponds to calculations. The inclusion of the second $\nu i_{13/2}$ alignment (BC) is shown by the dashed curve. (b) Band $\pi h_{11/2}[523]7/2^- \otimes \nu f_{7/2}[521]3/2^-$, fG, fH. The curves corresponds to calculations. The inclusion of the first $\nu i_{13/2}$ alignment (AB) is shown by the dashed curve. (c) Bands $\pi g_{7/2}[404]7/2^+ \otimes \nu i_{13/2}[642]5/2^+$, $\pi d_{5/2}[402]5/2^+ \otimes \nu i_{13/2}[642]5/2^+$, and $\pi h_{11/2}[523]7/2^- \otimes \nu h_{9/2}[523]5/2^-$. Calculations are shown with solid, long-dash and short-dash curves, respectively for the three bands. The latter has the first $\nu i_{13/2}$ alignment (AB) included.

crossing at $\hbar\omega \sim 0.25$ MeV blocked. These bands show the second $i_{13/2}$ (BC) crossing at $\hbar\omega \sim 0.35$ MeV. Both types of crossings are seen clearly in Fig. 4.

Most of the assignments of K (Table 2) correspond to the coupling with highest K. In the cases where this coupling is expected to be unfavoured at the band head [12] the high-K band may still become favoured over the low-K band when compared at the same (higher) spin, due to the additional rotational energy in the low-K band.

5.1. Bands with blocked AB crossing

5.1.1. Negative parity

The yrast band, fA, eA has been interpreted [4] as a $\pi[523]7/2^- \otimes \nu[642]5/2^+$ band, and this interpretation is confirmed in the present measurement by the firm spin and parity assignment, with the lowest state having $I^\pi = 6^-$. The crossing at $\hbar\omega \sim 0.35$ MeV corresponds to that expected for the BC crossing. The alignment and also the $B(\mathrm{M1})/B(\mathrm{E2})$ values agree with expectations, see also Section 6.5. Furthermore, the signature splitting develops with spin (frequency) resembling the observation for the $\pi[523]7/2^-$ bands, (e, f), in the odd ^{161,163}Tm isotopes [8,9].

The bands gA, gB have a signature splitting at low spin, and an inversion occurring at $\hbar\omega \sim 0.28$ MeV. An uncompleted BC crossing at $\hbar\omega \sim 0.41$ MeV is observed in the odd signature partner, which is known highest in spin. M1 cross-band transitions are observed in the spin region $I = 13$–17, only from odd to even spins. Furthermore, both signatures decay by dipole transitions of ~ 400 keV to bands dA, cA, which can be rather firmly assigned to the $\pi[411]1/2^+ \otimes \nu[642]5/2^+$ configuration, see below. This pattern resembles similar (E1) transitions between the bands $\pi[411]1/2^+$ and $\pi[541]1/2^-$ in odd-Z neighbours [8,9,15,16]. Taking also into account the alignment (Table 2) and the small values of $B(\mathrm{M1})/B(\mathrm{E2}) \sim 0.1$–$0.25\mu_N^2/e^2b^2$ in the spin range $I = 13$–$17\ \hbar$, the obvious candidate for the proton is $[541]1/2^-$, which is almost the only candidate for a second proton orbit with negative parity. The signature inversion, and the large BC-crossing frequency – which is shifted ~ 50 keV relative to bands fA, eA, bA, aA and dA, cA – is discussed in more detail in Subsection 6.2 below.

5.1.2. Positive parity

The lowest positive parity proton orbits are $[404]7/2^+$, $[411]1/2^+$ and $[402]5/2^+$, which are known in the neighbouring even-N Tm isotopes. These orbits are often found rather close in excitation energy with non-negligible interactions [15,16]. The most strongly populated positive parity bands with the $\nu[642]5/2^+$ orbital involved is bA, aA. The excitation energy, alignment and $B(\mathrm{M1})/B(\mathrm{E2})$ properties agree with expectations of $[404]7/2^+$ as the proton orbit, in accordance with the suggestion of Ref. [4]. It should be noted that the calculation of $B(\mathrm{M1})/B(\mathrm{E2})$ using [13] for the $[404]7/2^+$ band in odd-Z neighbours systematically underestimates the measured values, whereas particle-rotor calculations are found to give good agreement [16,17].

The bands dA, cA appear weakly coupled, with a signature splitting of $\Delta e' \sim 25$ keV at $\hbar\omega \sim 0.25$ MeV. They are therefore interpreted as $\nu[642]5/2^+$ coupled to $\pi[411]1/2^+$, which is the only positive parity proton orbit available at low excitation energy with a moderate signature splitting. This assignment is consistent with the observed alignment and very small values of $B(\mathrm{M1})/B(\mathrm{E2}) \sim 0.02$–$0.07\ \mu_N^2/e^2\mathrm{b}^2$, and in obvious disagreement with Ref. [5], in which the suggested parity was negative.

The bands lA, kA have the highest excitation energy and lowest alignment of these three pairs. The most characteristic property of the bands involving the $\pi[402]5/2^+$ orbit is the large $B(\mathrm{M1})/B(\mathrm{E2})$ values, which indeed agree with observations.

5.2. Bands with blocked BC crossing

5.2.1. Positive parity

The bands populated highest in spin are fG, fH, which become yrast at $I = 33\hbar$. These have not been observed earlier but are built on a known 5^+ state with an isomeric decay, for which the configuration $\pi[523]7/2^- \otimes \nu[521]3/2^-$ was suggested in Ref. [4]. The alignment and $B(\mathrm{M1})/B(\mathrm{E2})$ properties are consistent with this interpretation of the lowest bands with positive parity and an unblocked AB crossing. The $\nu[521]3/2^-$ orbit is expected to be slightly favoured compared to the $\nu[523]5/2^-$ orbit. In favour of this interpretation is that in ^{161}Er the bands GAB, HAB become favoured over band ABC at a similar spin as fGAB, fHAB compared to fABC, eABC [10].

A candidate for the $\pi[523]7/2^- \otimes \nu[523]5/2^-$ configuration is the pair, fE, fF, which are only known at $I > 21\hbar$ but clearly show the presence of an AB alignment and no BC crossing in the frequency region $0.3 < \hbar\omega < 0.4$ MeV. The observed $B(\mathrm{M1})/B(\mathrm{E2})$ values are consistent with this interpretation.

5.2.2. Negative parity

Possible negative parity configurations with a negative parity neutron require a positive parity proton. The lowest expected configuration of this type is $\pi[404]7/2^+ \otimes \nu[521]3/2^-$. The next lowest would be $\pi[404]7/2^+ \otimes \nu[523]5/2^-$, $\pi[411]1/2^+ \otimes \nu[521]3/2^-$ or $\pi[411]1/2^+ \otimes \nu[523]5/2^-$. The properties of the bands aH, bH, which like fE, fF are known to have an AB alignment and no BC crossing, are in good agreement with the former assignment. The upper limits on the $B(\mathrm{M1})/B(\mathrm{E2})$ values of $< 0.4\mu_N^2/b^2$ are in agreement with the calculation of $B(\mathrm{M1})/B(\mathrm{E2}) \sim 0.07\ \mu_N^2/\mathrm{b}^2$ for the high-K coupling of $\pi[404]7/2^+ \otimes \nu[521]3/2^-$, whereas the low-$K$ coupling would have $B(\mathrm{M1})/B(\mathrm{E2})$ values of the order of $0.65\ \mu_N^2/b^2$. Of the other possibilities the low-K coupling of $\pi[411]1/2^+ \otimes \nu[521]3/2^-$ with expected $B(\mathrm{M1})/B(\mathrm{E2})$ values of $0.002\ \mu_N^2/\mathrm{b}^2$ cannot be excluded. The observations of stretched E2 transitions to bands fA, eA with $K = 6$ makes the assignment of aH, bH to the high-K (= 5) coupling of the lowest expected configuration, $\pi[404]7/2^+ \otimes \nu[521]3/2^-$, most likely.

6. Discussion

The present data contain spectroscopic information to a high degree of detail. Based on this it is possible to address (i) questions related to the high-frequency alignment processes, (ii) the role of residual interactions as revealed in signature properties of specific configurations as well as (iii) electromagnetic (M1 and E1) transition probabilities within and between specific bands.

6.1. High-spin properties, $\hbar\omega_c$ at high frequencies

The band structures which are established highest in spin are fG, fH and fA, eA with positive and negative parity, respectively. They are also lowest in excitation energy. These bands have the $\pi h_{11/2}[523]7/2^-$ configuration in common. Except for band eA, an upbend at $\hbar\omega \sim 0.6$ MeV is observed in these bands. To understand the nature of this crossing, common to fG, fH and fA, it is useful to consult neighbouring nuclei. Several bands in the isotopes ^{160,161,162}Er [18–20], and the yrast $\pi h_{11/2}[523]7/2^-$ band, f, in ^{163}Tm [9], are known to sufficiently high spin. The first proton alignment corresponding to (ef) appears consistently at $\hbar\omega \sim 0.47$ MeV in the configurations A(BC), G(AB) and H(AB) in ^{161}Er and in AB and AG (BC) in ^{160,162}Er with no additional crossings up to $\hbar\omega \sim 0.65$ MeV in any of these bands, except for the last state at $I = 50$ in ^{160}Er, which might be lowered due to a possible band termination [20]. In ^{163}Tm the band, f, has an upbend at $\hbar\omega \sim 0.61$ MeV whereas the partner band, e, is only known to $\hbar\omega \sim 0.51$ MeV.

If the second pair of $h_{11/2}$ quasiprotons are labelled (i, j), then the second proton crossing will, for a configuration containing e or f, correspond to (fi) or (ej), respectively. Both of these crossings will be blocked in the Er bands which all have e and f aligned above $\hbar\omega \sim 0.47$ MeV. From cranked shell model (CSM) calculations [21] we expect the (ej) and (fi) alignments to occur at $\hbar\omega \sim 0.38$ and ~ 0.49 MeV, respectively. For the neutron AB alignment the expected crossing frequency is $\hbar\omega \sim 0.24$ MeV which is somewhat smaller than the observed value of $\hbar\omega \sim 0.28$ MeV. Likewise, the expected frequency of the proton (ef) alignment is 0.37 MeV compared to the observed frequency of $\hbar\omega \sim 0.47$ MeV. With the systematic underestimate from the CSM calculations in mind we suggest that the observed upbend in bands fG, fH and fA, together with that observed in band f in ^{163}Tm, could be compatible with the second $h_{11/2}$ crossing, (ej). This scenario also explains the non-observation of an upbend in band eA(BC), since the second $h_{11/2}$ crossing, (fi) is expected at a higher frequency. The gradual alignment gains in the frequency range $0.35 < \hbar\omega < 0.5$ in bands fG, fH and possibly in bands fE, fF which both have the AB neutrons aligned, but not in bands fA, eA with the BC neutrons aligned, might be due to a CD neutron alignment, although this would be expected at somewhat higher frequency ($\hbar\omega > 0.5$ MeV).

6.2. Inversion in $\pi[541]1/2^- \otimes \nu[642]5/2^+$

The present data provide one of the first examples of a semi-decoupled band built on the $\pi h_{9/2}[541]1/2^- \otimes \nu i_{13/2}[642]5/2^+$ configuration in which the spin assignment is firm. For this configuration the favoured signature of both constituents are $\alpha = +1/2$, and therefore, the expected favoured signature is $\alpha = 1$. The data show that the signature is clearly inverted with $\alpha = 0$ favoured at lower spins up to $I \approx 18\hbar$ (see Fig. 3).

Signature inversions are common features in other two-quasiparticle bands in odd–odd nuclei. The configuration $\pi h_{11/2} \otimes \nu i_{13/2}$ is inverted at low spins in the lighter Tb, Ho and Tm isotopes (see Ref. [22] for a summary). Possible causes are triaxial

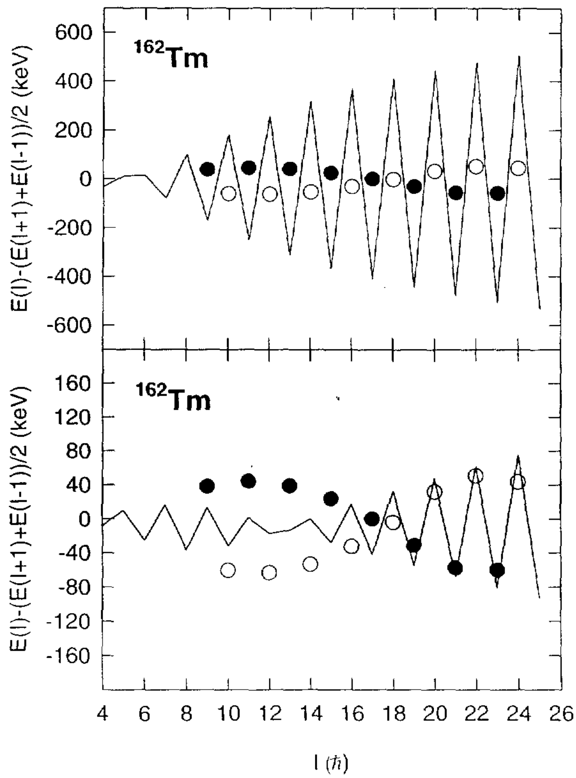

Fig. 6. Results of the particle-rotor calculations on the energy staggering for the band $\pi h_{9/2}[541]1/2^- \otimes \nu i_{13/2}[642]5/2^+$ compared to experiment. The lower panel has the V_{pn} included and a decreased Y-scale.

shapes [23] and Coriolis effects [24,25,28] which may explain signature inversion for $I < j_\pi + j_\nu$. Proton–neutron interactions [26] have been invoked to explain such inversions and it was shown recently in Ref. [27] that p-n interactions can also explain signature inversion effects in $\pi h_{9/2} \otimes \nu i_{13/2}$ configurations over a wide range of the rare-earth region.

The observed staggering of the $\pi[541]1/2^- \otimes \nu[642]5/2^+$ band, gA, gB is presented in Fig. 6. In the upper part of the figure the data are compared to expectations from particle-rotor model calculations by the code of Ragnarsson and Semmes [29] with $(\varepsilon_2, \varepsilon_4) = (0.27, 0)$ and axial symmetry, $\gamma = 0$. Like the CSM, they predict the signature $\alpha = 1$ to be favoured, and are out of phase with the data. Triaxiality with $\gamma = \pm 10°$ is also not able to repair the staggering phase.

In Fig. 6b the experimental staggering is compared to particle-rotor calculations including a residual proton–neutron interaction of the form

$$V_{pn} = \sqrt{8\pi^3} \left(\frac{\hbar}{m\omega} \right)^{3/2} \delta\left(\boldsymbol{r}_p - \boldsymbol{r}_n\right) \left(u_0 + u_1 \sigma_p \cdot \sigma_n\right) \tag{4}$$

This interaction has also been employed to understand signature splitting effects in the $A = 130$ and 150 mass regions [26,29], in connection with $\pi h_{11/2} \otimes \nu h_{11/2}$ and $\pi h_{11/2} \otimes \nu i_{13/2}$ bands. In the Tm region, reasonable values for the parameters u_0 and u_1 were found to be $u_0 = -4.95$ MeV and $u_1 = -0.55$ MeV [27]. Using these parameters, the residual interaction reproduces the staggering phase with a change at $I \sim 13\hbar$ compared to the observed phase change at $I \sim 18\hbar$.

The mechanism by which V_{pn} causes the inversion is discussed in Ref. [27], and further details shall be given in a report on ^{164}Tm [30]. It can be related to a difference in the particle–hole character of the odd spin states compared to the even spin states, and the sign of the interaction matrix elements.

It should be added that in Ref. [31] it is shown empirically, that deformation changes together with the proton–neutron interaction, (which explains a similar signature inversion in ^{174}Ta), can account for the increased crossing frequency associated with the alignment of $i_{13/2}$ neutrons in the $\pi[541]1/2^-$ band of odd-Z neighbours [32]. Presumably, V_{pn} also contributes to the delayed BC crossing observed in the band gA. However, the empirical analysis of routhians performed [31] for ^{173,174}Ta is less reliable here, due to severe deformation changes between $N = 92$ to $N = 94$ Tm isotopes.

6.3. Interactions at band crossings

The bands observed in the present experiment are subject to several cases of crossings with measured E2 decay branching which, as described in Section 4, have provided independent information useful in the spin and parity determinations. There are 4 cases of isolated crossings in which the interaction is limited to at most 2 neighbouring states, I and $I - 2$. At such crossings an interaction strength may be extracted from the observed energy differences and E2 branching intensities rather independent of the particular modeling of the unperturbed bands provided that the measured energies in the crossing region are well reproduced. The technique of analysing interactions between up to 3 bands follows the procedure given in Ref. [33] and references therein. This procedure gives values in agreement with the simpler 2-band analysis of Ref. [34].

The crossings are illustrated in Fig. 7, which is an expansion of part of Fig. 3 for the positive parity bands. The parameters characterizing the bands together with the extracted interaction strength are listed in Table 3. It should be noted that some of these interactions, like dA ⇔ fE and aA ⇔ fF, cause irregularities in the alignment plot of the positive parity bands in Fig. 4, which are removed in the unperturbed bands. In one case, bA ⇔ dA, no cross band transitions were observed, but a rather low upper limit of $V < 1.5$ keV could be given from the closest level distance at $I = 20\hbar$.

The bands involved are all subject to alignment processes of the most easily alignable $i_{13/2}$ quasineutrons, and Table 3 includes the aligning quasineutrons, AB or BC. Cases where the crossing occurs close to the 'middle' of the alignment process are given in parenthesis. As can be seen from Table 3, the data sample specific configurations in various combinations, which also provides a variation in the differences in the change in the projection ΔK on the symmetry axis and Δi on the rotation axis. The spin I at which the crossings occur vary between 17 and 26. The extracted values of the strength

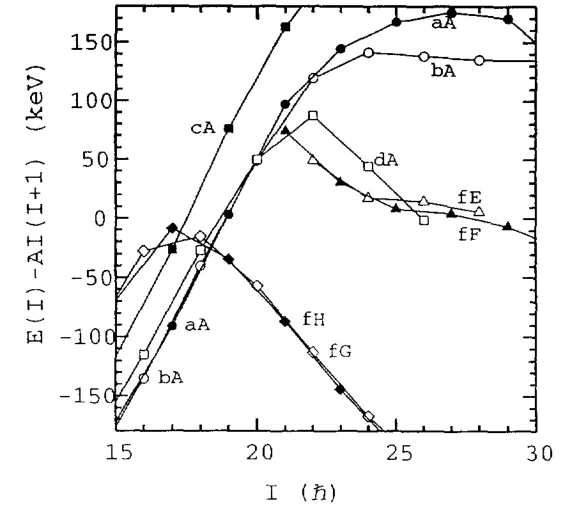

Fig. 7. Expanded picture relative to Fig. 3 of excitation energy versus spin for selected positive parity bands in ^{162}Tm to illustrate the observed band crossings.

Table 3
Interactions between rotational bands in ^{162}Tm. Cases where both bands are known below and above the crossing are included. For the classification of assignments see Table 2. Orbitals changed in the interaction are underlined. Partly aligned pairs of $i_{13/2}$ quasineutrons are given in parentheses

	Interacting bands				Strength V	$\sim \Delta K$	~Spin	$\sim \Delta i$
K_1	Label$_1$	$\Longleftrightarrow$	Label$_2$	K_2	keV	$\hbar$	$\hbar$	$\hbar$
6	bA(BC)	$\Longleftrightarrow$	dA(BC)[a]	2	<1.5	4	20	0.6
5	fG(AB)	$\Longleftrightarrow$	dA	2	5(1)	3	18	2.0
5	fH(AB)	$\Longleftrightarrow$	cA	2	5(1)	3	17	1.9
5	fFAB	$\Longleftrightarrow$	aA(BC)	6	11(1)	1	21	2.8
6	fEAB	$\Longleftrightarrow$	dABC	2	7(1)	3	26	0.5

[a] No cross band transitions are observed in this case

V are fairly small, between 1.5 and 11 keV.

Of the interactions given in Table 3, the first differs from the rest in that the neutron configurations A(BC) are unchanged and only the proton is changed from d, $d_{3/2}[411]1/2^+$, to b, $g_{7/2}[404]7/2^+$. One can therefore compare the interaction to the observation of the same crossing in the odd-Z neighbours. This interaction can be estimated [9] in ^{163}Tm to be < 5 keV, and 5.0 (0.5) keV in both of the heavier ^{165,167}Tm [15,35] at $I \sim 9.5\hbar$. In the presence of A(BC) quasineutrons and at the increased spin of $20\hbar$ this interaction is apparently decreased. The expected frequency (spin) dependence for the interaction of two Nilsson configurations would most naturally be an increase due to increased Coriolis interaction, but other variables such as pairing could also play a role. [9]. An explanation might be found in the K-coupling. As listed in Table 2, the K-coupling is assumed to be K_ν - K_π = 2, which is also favoured

Table 4
Possible crossings between quasiparticle bands, schematically. (In reality, the excitation energies have to be comparable, and aligning quasiparticles will in many cases also be present)

Nucleus	Interacting bands			ΔK
Even–even	AF, AE	$\Longleftrightarrow$	af, ae	2
Odd Z	a, b	$\Longleftrightarrow$	fAE, eAE	5
Odd Z	e, f	$\Longleftrightarrow$	bAE, aAE	5
Odd N	A, B	$\Longleftrightarrow$	Fae, Eae	7
Odd N	E, F	$\Longleftrightarrow$	Aaf, Aae	7
Odd–odd	aF, aE	$\Longleftrightarrow$	Af, Ae	0

and gives rise to $\Delta K = 4$ at the dA $\Leftrightarrow$ bA crossing, compared to the odd-proton case d$\Leftrightarrow$b where $\Delta K = 7/2 - 1/2 = 3$.

The other 4 interactions have strengths varying between 5 and 11 keV. It is interesting to compare the interactions from the present odd–odd data to interactions sampling the same configurations in other combinations which could be present in neighbouring even–even, odd-N and odd-Z nuclei. The lowest 2-quasineutron and 2-quasiproton configurations in even–even nuclei are AF, AE and af, ae, when excluding the aligned pairs like AB and ef, etc. Bands built on these two configurations are found in ^{162,164}Er [19,36], and recently the combined 4-quasiparticle band AEae, AEaf has been found in ^{164}Er [37]. In odd nuclei the same 2-quasiparticle configuration forms the basis for the lowest 3-quasiparticle bands. Interactions between these possible lowest multi-quasiparticle configurations are listed schematically below in Table 4. They comprise a variety of combinations of the same quasiparticles which basically should have comparable interactions provided that the Fermi level is stable. On the other hand, one could expect a change in ΔK to influence the interaction. In reality this simplified picture does not hold since the bands need comparable excitation energies and more quasiparticles which are often aligned will be present.

In ^{163}Tm the 3-quasiparticle bands eAE, fAE have a complicated crossing with bands a, b and c, d. Yet the interactions aAB $\Leftrightarrow$ fAE at $I \sim 39/2\hbar$ can be estimated to be $V \sim 6.6$ keV, and an upper limit of $V < 2.5$ keV can be given for the d(AB) $\Leftrightarrow$ eAE interaction from the closest level distance at $I = 31/2\hbar$. For the odd-N neighbour a recent analysis of the band structures in ^{163}Er [38] has revealed a multitude of band crossings. Only few involve the quasiprotons ae, and of these only EAC $\Leftrightarrow$ eaA with a strength of 1–2 keV has configurations comparable to the present data.

Although small, these values have measurable effects on the band structures and decay pattern. When inspecting the constituent quasiparticles, one is faced with interactions which have to mediate changes of both signature and parity of quasiprotons and quasineutrons simultaneously. One may therefore also have to invoke proton–neutron interaction unless coupling to collective octupole degrees of freedom will provide an explanation, as suggested in Ref. [38].

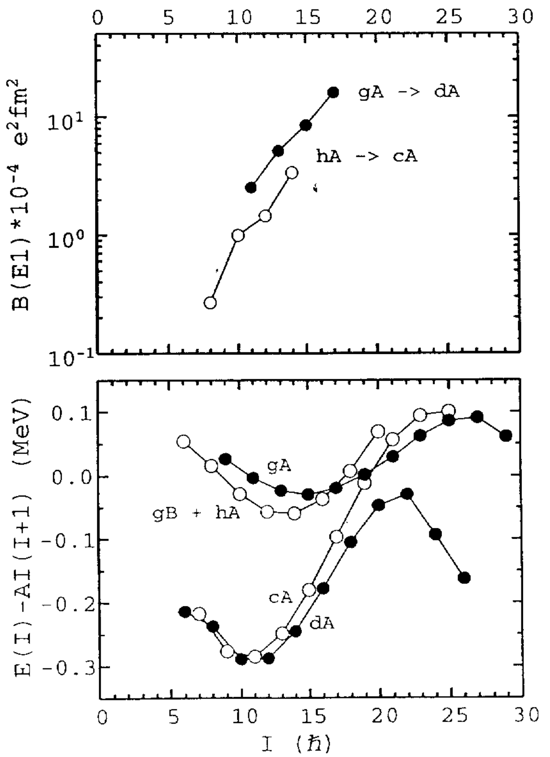

Fig. 8. (a) Experimental values of B(E1) for transitions from bands $\pi h_{9/2}[541]1/2^- \otimes \nu i_{13/2}[642]5/2^+$, gA, gB, to bands $\pi d_{3/2}[411]1/2^+ \otimes \nu i_{13/2}[642]5/2^+$, dA, cA. (b) The excitation energy relative to a rigid rotor for the same bands as (a).

6.4. Enhanced E1 strength in $\pi[541]1/2^- \otimes \nu[642]5/2^+ \to \pi[411]1/2^+ \otimes \nu[642]5/2^+$

The $\Delta I = 1$ E1 decay observed from both signatures of the $\pi[541]1/2^- \otimes \nu[642]5/2^+$, gA, gB, configuration to the opposite signatures in the $\pi[411]1/2^+ \otimes \nu[642]5/2^+$ configuration, dA, cA, is characteristic for the two quasiproton configurations for which such E1 decays are observed in a number of surrounding odd-Z nuclei [8,9,15–17,35]. The enhanced E1 matrix elements have been interpreted in terms of coupling to octupole vibrational degrees of freedom [39]. An estimate of the B(E1) strength can be obtained from the relative intensity of the $I \to I-1$ E1 transition and $I \to I-2$ E2 rotational in-band transition, for which the strength is assumed to correspond to a transition quadrupole moment of 6.5b. We can conveniently compare the present E1 strength shown in Fig. 8 to the observations in ^{165}Tm, in which E1 transitions are observed in a rather large spin range [15]. In the odd-Z case the comparable transitions characterized as $[541]1/2^-, \alpha = -1/2 \to [411]1/2^+, \alpha = +1/2, (h \to c)$ and $[541]1/2^-, \alpha = +1/2 \to [411]1/2^+, \alpha = -1/2, (g \to d)$ have B(E1) values in the order of 1–$2 \times 10^{-3} e^2\text{fm}^2$ [15], representing an enhancement of several orders of magnitude over expectations from calculations for a pure dipole strength based on an effective charge of $e_{\rm eff} = 0.2e$ [39].

In the present odd–odd case, the E1 transitions are observed between the bands characterized as gA → dA and gB → cA. Of these there is a large difference in strength, namely, B(E1) values for gA → dA are ~ 2–2.5 times larger than the B(E1) values for gB → cA in the spin range where both types of transitions are observed. In the quasiparticle picture the transitions gB → cA are not possible, since the E1 operator connects states of opposite parity and therefore cannot change B into A. Assuming that the E1 strength in the latter case represents hA → cA and not gB → cA the observed strength suggests that there is an admixture of ~ 20–25% of hA in the band interpreted as gB for spins $I = 12$–$14\hbar$. Such a mixing can result from an interaction between the two structures for which the unperturbed bands are expected to be separated by the difference in signature splitting between the neutron $i_{13/2}$ bands A, B, and the proton $h_{9/2}$ bands, g, h, approximately, which is expected to be of the order of 100–200 keV. A systematic analysis of these signature splittings can be found in Refs. [40,41].

The structure of the two bands, hA and gB, is characterized by a signature change within a positive orbital, A, B, and a negative parity proton orbital, g, h, simultaneously. This kind of interaction can be traced to the recoil term of the hamiltonian for the two particles coupled to a rotor, and estimated [42] to depend on the signature splitting and alignment of the two orbitals as well as the moment of inertia. Such interactions can indeed be rather large, of the order of ~ 100 keV if both of the orbitals have a large signature splitting like in the present case. An unperturbed energy difference of 100–200 keV could therefore produce admixed amplitudes in agreement with observations. The observed difference in E1 strength for the two signatures is thus in qualitative agreement with the interpretation of these bands and provides independent information on the wave function of the even-spin members of the semi-decoupled $\pi h_{9/2}[541]1/2^- \otimes \nu i_{13/2}[642]5/2^+$ band structures discussed in Subsection 6.2.

6.5. *M1 transition strength in the* $\pi[523]7/2^- \otimes \nu[642]5/2^+$ *band*

The present results include experimental values of B(M1)/B(E2) to quite high spin values, $I = 34\hbar$, in the negative parity yrast bands, fA, eA. The corresponding values for the $\pi h_{11/2}[523]7/2^-$ band have been measured up to 51/2 and 59/2 $\hbar$ in ^{161}Tm [8] and ^{163}Tm [9], respectively. In the present data for the band in ^{162}Tm coupled to an $i_{13/2}$ quasineutron a signature splitting in B(M1)/B(E2) sets in gradually at $I \sim 15\hbar$ and becomes significant in the range $20 < I < 30$. For $I > 30\hbar$ the errors are too large to allow an extraction of a well defined splitting. In single-quasiparticle bands built on high-j orbits a simple relationship exists between the relative signature splitting, $\Delta e'$, in excitation energy, routhian, e', and ΔB(M1) in the M1 cross-band transition probabilities. Both effects can be traced to the same origin, namely the Coriolis induced amplitude of $K = 1/2$ in the wave function which increases with rotational frequency. The expected relation for an axially symmetric nucleus is

$$\frac{\Delta B(\mathrm{M1})}{\langle B(\mathrm{M1})\rangle} = \frac{4\Delta e'/\hbar\omega}{1+(\Delta e'/\hbar\omega)^2} \tag{5}$$

and a divergence from this relationship has been analysed in terms of a divergence from axial symmetry, i.e. $\gamma \neq 0$ [43]. It can be justified to assume that the signature splitting in $B(\mathrm{M1})/B(\mathrm{E2})$ is mainly due to a signature dependence in $B(\mathrm{M1})$. In the lighter odd-Z rare earth nuclei the $h_{11/2}$ band has a splitting much larger than expected from CSM calculations, but becomes in agreement with expectations for frequencies above the AB neutron crossing. See Ref. [8] for a discussion of the systematics of this feature in the low spin range below the AB crossing. In the fA, eA bands in odd-odd ^{162}Tm we have one $i_{13/2}$ quasineutron, A, in addition to e, f in the full frequency range, and the signature splitting seems to develop in accordance with the expectations for an $h_{11/2}$ quasiproton. If the $i_{13/2}$ quasineutron, A, apart from having forced the nucleus into an axially symmetric shape, behaves as a spectator, then it can be justified to test the data on the above relation. It seems that we have qualitative agreement, namely the left-hand side and right-hand side of Eq. (5) have values of ~ 0.4 and ~ 0.36, respectively for spins $I = 22$–$26\hbar$. This result is comparable to a ratio of 1.16 between the left-hand side and right-hand side of Eq. (5) found for the neighbouring isotope, ^{163}Tm [9] at $I \sim 27\hbar$. It should be noted, that the calculated values of $B(\mathrm{M1})/B(\mathrm{E2})$ shown in Fig. 5a has no signature effect included. The difference in spin dependence of experiment and calculation might be due to a decrease in Q_0 with spin.

7. Summary and conclusion

The present detailed spectroscopy on an odd-odd nucleus has expanded our knowledge to the band structures in ^{162}Tm considerably. Altogether 16 bands based on eight Nilsson couplings of the lowest quasiprotons and neutrons have been identified, and some of them were established high enough in spin to reach the second $h_{11/2}$ proton crossing. The observation of several band crossings has provided severe restrictions to help a firm spin and parity assignment of the bands, which all except for one pair are interconnected.

Various phenomena which can be related to residual neutron-proton interactions have been in focus. In particular, the signature inversion in the bands $\pi[541]1/2^- \otimes \nu[642]5/2^+$, based on the lowest $h_{9/2}$ quasiproton and $i_{13/2}$ quasineutron, respectively. A residual pn interaction in the form of a delta function can explain the observed (spin-dependent) shift in energy of the band with $\alpha = 1$. This interaction is also most likely active in the three-quasiparticle bands $\pi h_{9/2} \otimes \nu i^2_{13/2}$, which in odd-$Z$ neighbours have a delayed crossing with the $\pi h_{9/2}$ band.

Another type of interaction could be traced from the intensity of E1-transitions connecting bands with opposite signature of the structure $\pi[541]1/2^- \otimes \nu[642]5/2^+ \rightarrow \pi[411]1/2^+ \otimes \nu[642]5/2^+$, i.e. gA $\rightarrow$dA and gB $\rightarrow$ cA. The latter is forbidden because of the E1 selection rule, showing that we are dealing with a mixture of gB and hA, which in the case of two orbitals with a large signature splitting can be as large as up to 100 keV, mediated by the recoil term in the coupling of two particles to a rotor.

In addition to these larger band interactions which cause considerable shifts in energies smaller interactions reveal themselves at the many band crossings at which E2 cross band transitions are observed. The extracted interaction strength of the order of a few keV are consistent with similar observations for bands based on the same constituent quasiparticles in different combinations in neighbouring odd-N and odd-Z nuclei. Some dependence on the differences in K may exist.

Acknowledgements

Fruitful discussions with I. Hamamoto are highly acknowledged. This work was supported by the Danish Natural Science Foundation, the Nordic Committee for Accelerator Based research, NorFa, the NORDBALL collaboration and the Spanish CICYT (project PB95-0533) (J.M.E.).

References

[1] B. Herskind, Nucl. Phys. A 447 (1986) 395c;
G. Sletten, J. Gascon and J. Nyberg, Proc. Int. Conf. on the Spectroscopy of heavy Nuclei, Crete 1989. IOP Conf. Series No 105 (IOP Publishing, Bristol) p. 125.
[2] D.C. Radford, Nucl. Inst. and Meth. in Phys. Res. A 361 (1995) 297.
[3] B. Million, S. Leoni, A. Bracco, J. Moretti, S. Frattini, P. Bosetti, F. Camera, M. Mattiuzzi, B. Herskind, R.A. Bark, I. Bearden, G.B. Hagemann and H.J. Jensen, Phys. Lett. B 415 (1997) 321.
[4] S. Drissi, J.-Cl. Dousse, V. Ionescu, J. Kern, J.-A. Pinston and D. Barnéoud, Nucl. Phys. A 466 (1987) 385.
[5] S. André, D. Barnéoud, C. Foin, J. Genevey, J.-A. Pinston, B. Haas, J.P. Vivien and A.J. Kreiner, Z. Phys. A 333 (1989) 247.
[6] A. Bohr and B. R. Mottelson, Nuclear Structure, Vol. 2 (W.A. Benjamin, New York, 1975).
[7] F.W.N de Boer, P.F.A. Goudsmit, P. Kololewijn and B.J. Meyer, Nucl. Phys. A 169 (1971) 577.
[8] A.G. Smith, R. Chapmann, D.C. Clarke, J. Copnell, S.J. Freeman, F. Khazaie, G.S. Li, J.S. Lisle, J.N. Mo, C. Tenreiro, D.M. Thompson, G.J Yuan, J. Espino and G.B. Hagemann, Nucl. Phys. A 587 (1995) 150.
[9] H.J. Jensen, G.B. Hagemann, P.O. Tjøm, S. Frauendorf, A. Ataç, M. Bergström, A. Bracco, A. Brockstedt, H. Carlsson, P. Ekström, J.M. Espino, B. Herskind, F. Ingebretsen, J. Jongman, S. Leoni, R.M. Lieder, T. Lönnroth, A. Maj, B. Million, A. Nordlund, J. Nyberg, M. Piiparinen, H. Ryde, M. Sugawara and A. Virtanen, Z. Phys. A 340 (1991) 351;
H.J Jensen, private communication (1997).
[10] J.D. Garrett, G.B. Hagemann, B. Herskind, J. Bacelar, R. Chapman, J.C. Lisle, J.N. Mo, A. Simcock, J.C. Willmott and H.G. Price, Phys. Lett. B 118 (1982) 297.
[11] J. Kownacki, J.D. Garrett, J.J. Gaardhøje, G.B. Hagemann, B. Herskind, S. Jönsson, N. Roy, H. Ryde and W. Walus, Nucl. Phys. A 394 (1983) 269.
[12] C.J. Gallagher and S.A. Moszkowski, Phys. Rev. 111 (1958) 1282.
[13] F. Dönau, Nucl. Phys. A 471 (1987) 469.
[14] S. Raman, C.H. Malarkey, W.T. Milner, C.W. Nestor Jr. and P. Stelson, Atomic Data and Nucl. Data Tables 36 (1987) 1.
[15] H.J. Jensen, Thesis, University of Copenhagen 1996 and H.J. Jensen et al., to be published.
[16] S. Ogaza, J. Kownacki, M.P. Carpenter, J. Gascon, G.B. Hagemann, Y. Iwata, H.J. Jensen, T. Komatsubara, J. Nyberg, G. Sletten, P.O. Tjøm, W. Waluś and I. Hamamoto, Nucl. Phys. A 559 (1993) 100.
[17] H. Carlsson, R.A. Bark, L.P. Ekström, A. Nordlund, H. Ryde, S.J. Freeman, G.B. Hagemann, H. J. Jensen, H. Schnack-Petersen, F. Ingebretsen, P.O. Tjøm, T. Lönnroth and M.J. Piiparinen, Nucl. Phys. A 592 (1995) 89.
[18] J. Simpson, M.A. Riley, A.N. James, A.R. Mokhtar, H.W. Cranmer-Gorden, P.D. Forsyth, A.J. Kirwan, D. Howe, J.D. Morrison and J.F. Sharpey-Shafer, J. Phys. G 13 (1987) L235.

[19] M.A. Riley, J.W. Roberts, J. Simpson, A. Alderson, I. Ali, M.A. Bentley, A.M. Bruce, R. Chapman, D.M. Cullen, P. Fallon P.D. Forsyth, J.C. Lisle, J.N. Mo and J.F. Sharpey-Shafer, J. Phys. G 16 (1990) L67.
[20] J. Simpson, private communication, (1997).
[21] R. Bengtsson, S. Frauendorf and F.R. May, At. Data and Nucl. Data Tables 35 (1986) 15.
[22] T. Komatsubara et al., Nucl. Phys. A 557 (1993) 419c.
[23] R. Bengtsson, J.A. Pinston, D. Barnéoud, E. Monnard and F. Schussler, Nucl. Phys. A 389 (1982) 158.
[24] A.J. Kreiner and M.A.J. Mariscotti, J. Phys. G 6 (1980) L13.
[25] A.K. Jain, J. Kvasil, R.K. Sheline and R.W. Hoff, Phys. Lett. B 209 (1988) 19.
[26] N. Tajima, Nucl. Phys. A 572 (1994) 365.
[27] R.A. Bark, J.M. Espino, W. Reviol, P.B. Semmes, H. Carlsson, I.G. Bearden, G.B. Hagemann, H.J. Jensen, I. Ragnarsson, L.L. Riedinger, H. Ryde and P.O. Tjøm, Phys. Lett. B 406 (1997) 193; B 416 (1998) 453.
[28] I. Hamamoto, Phys. Lett. B 235 (1990) 221.
[29] P.B. Semmes and I. Ragnarsson, Conf. High Spin Physics and Gamma-soft Nuclei, Pittsburg, September 1990 (World Scientific, Singapore, 1991) p. 500; Conf. on Future Directions in Nuclear Physics with 4π Detection Systems of the Generation, Strasbourg, March 1991 (AIP, New York, 1992) p. 556.
[30] W. Reviol, L.L. Riedinger, X.Z. Wang, J.-Y. Zhang, H.J.Jensen, G.B. Hagemann, R.A. Bark, P.O. Tjøm, S. Leoni, T. Lönnroth, H. Schnack-Petersen, T. Shizuma, J. Wrzesinski, P.B. Semmes and I. Ragnarsson, to be published.
[31] R.A. Bark, H. Carlsson, S.J. Freeman, G.B. Hagemann, F. Ingebretsen, H.J. Jensen, T. Lönnroth, M.J. Piiparinen, I. Ragnarsson, H. Ryde, H. Schnack-Petersen, P.B. Semmes, P.O. Tjøm, Nucl. Phys. A 630 (1998) 603.
[32] H.J. Jensen and R.A. Bark, Acta Phys. Pol. B 26 (1995) 271.
[33] R.A. Bark, G.B. Hagemann, B.Herskind, H.J. Jensen, W. Korten, J. Wrzesinski, H. Carlsson, M. Bergström, A. Brockstedt, A. Nordlund, H. Ryde, P. Bosetti, S. Leoni, F. Ingebretsen and P.O. Tjøm, Nucl. Phys. A 591 (1995) 265.
[34] G.B. Hagemann and I. Hamamoto, Phys. Rev. C 46 (1992) 838.
[35] H.J. Jensen, P.O. Tjøm, D. Foltescu, A. Gadea, W. Gast, R.M. Lieder, R. Menegazzo, D.R. Napoli, Z. Podolyak and C. Ur, to be published and private communication (1997).
[36] C.A. Fields, K.H. Hicks, R.A. Ristinen, F.W.N. de Boer, L.K. Peker, R.J. Peterson and P.M. Walker, Nucl. Phys. A 422 (1984) 215.
[37] R.A. Bark, P. Bosetti, G.B. Hagemann, A. Brockstedt, H. Carlsson, L.P. Ekström, A. Nordlund, B. Herskind, S. Leoni, A. Bracco, F. Camera, S. Frattini, M. Mattiuzzi, B. Million, C. Rossi-Alvarez, G. de Angelis, D. Bazzacco, S. Lunardi and M. De Poli, Z. Phys. A 359 (1997) 5.
[38] G.B. Hagemann, H. Ryde, P.Bosetti, A. Brockstedt, H. Carlsson, L.P. Ekström, A. Nordlund, R.A. Bark, B. Herskind, S. Leoni, A. Bracco, F. Camera, S. Frattini, M. Mattiuzzi, B. Million, C. Rossi-Alvarez, G. de Angelis, D. Bazzacco, S. Lurnardi and M. de Poli, Nucl. Phys. A 618 (1997) 199.
[39] G.B. Hagemann, I. Hamamoto and W. Satuła, Phys. Rev. C 47 (1993) 2008.
[40] W.F. Mueller, H.J. Jensen, W. Nazarewicz, W. Reviol, L.L. Riedinger, R. Wyss, C.-H. Yu and J.-Y. Zhang, Phys. Rev. C 50 (1994) 1901.
[41] H.J. Jensen, W.F. Mueller, W. Nazarewicz, W. Reviol, L.L. Riedinger and J.-Y. Zhang, Acta Phys. Pol. B 28 (1997) 169, and to be published.
[42] I. Hamamoto, Proc. Workshop on Nuclear Structure in the Era of New Spectroscopy, The Niels Bohr Institute, Oct. 1989, p 323.
[43] G.B. Hagemann and I. Hamamoto, Phys. Rev. C 40 (1989) 2862.